Contents

1 Introduction

Quantum Chromodynamics (QCD) is the theory that describes the dynamics of the strong force, which acts upon fundamental particles known as quarks, with interactions mediated by gluons. Unlike other forces, the interaction strength of the strong force increases with distance. While perturbation theory is commonly employed to study other forces, such as electromagnetism [1], it proves inadequate for QCD at low energies due to the self-interacting nature of gluons [2].

To overcome this limitation, a theoretical framework known as Lattice QCD is used. This theoretical framework discretizes the space-time, enabling the study of the low-energy properties of strong interactions. Specifically, it is instrumental in studying phenomena such as hadron scattering and resonances [3]. The primary focus of this project is the extraction of phase shifts in partial waves that describe meson-meson scattering below inelastic thresholds, specifically the $\pi\pi$ scattering process.

Throughout this work, natural units are employed, where $\hbar = 1; c = 1$ with energies expressed in terms of MeV.

2 Lattice QCD in a finite volume at stationary frame

2.1 Theory

The Lattice QCD considers a square lattice box of volume L^3 with periodic boundary conditions and spatial spacing a. For two particles in such a lattice, known as two-particle states on a torus [4], the total three-momentum satisfies the periodic boundary condition:

$$\mathbf{P} = \mathbf{p_1} + \mathbf{p_2} = \frac{2\pi}{L}\mathbf{n}, \quad \mathbf{n} \in \mathbb{Z}^3 \tag{1}$$

The goal is to derive the relationship between the total energy E of the two-particle system in the box and the resonance behavior. This relation is straightforward in the non-interacting case. However, in the interacting case, the total energy E can be determined using partial wave analysis, where the energy spectrum is decomposed into constituent angular-momentum components. The total energy E is related to the scattering phase shifts δ_l in the l-th partial wave. In practice, the total energy E is obtained via the lattice simulation based on gauge field configurations encoding the quark interactions [5], and the scattering phase shifts δ_l are extracted from the energy spectrum to study the interaction between particles, such as resonances.

2.1.1 Non-interacting case

Assuming that two particles are not interacting, the momentum of the individual particles satisfies the periodic boundary condition:

$$\mathbf{p}_i = \frac{2\pi}{L}\mathbf{n}_i, \quad \mathbf{n}_i \in \mathbb{Z}^3 \text{ for } i = 1, 2 \tag{2}$$

The total momentum and energy are then the sums of the individual momenta and energies, respectively:

$$\mathbf{P} = \mathbf{p}_1 + \mathbf{p}_2 \tag{3}$$

$$E = \sqrt{m_1^2 + |\mathbf{p}_1|^2} + \sqrt{m_2^2 + |\mathbf{p}_2|^2} \tag{4}$$

where $m_{1,2}$ are the masses of the two particles. The total energy E is quantized due to the periodic boundary condition, as the momenta $\mathbf{p}_i$ are restricted to discrete values determined by the lattice size L.

2.1.2 Interacting case

Consider two spinless bosons of mass $m_{1,2} = m$ with zero total momentum. The two-particle states are described by the wave function $\psi((r))$, where $\mathbf{r} = \mathbf{x}_1 - \mathbf{x}_2$ is the relative position of the two particles. Their interaction is assumed to have a finite range of R.

$$V(\mathbf{r}) \begin{cases} = 0 & \text{for} \quad |\mathbf{r}| > R \\ \neq 0 & \text{for} \quad |\mathbf{r}| \leq R \end{cases} \tag{5}$$

where $|\mathbf{r}|$ represents the magnitude of the relative position vector. The Hamiltonian for this system is given by

$$H = -\frac{1}{2m}\Delta + V(\mathbf{r}). \tag{6}$$

where Δ is the Laplacian operator with respect to $\mathbf{r}$ and $\mu = m/2$ is the reduced mass of the system [4]. Due to finite ranged interaction, it suffices to consider the system inside a finite extent given the interaction region is contained [6].

In the region beyond the range of interaction, the solutions to the Schrödinger equation obey the Helmholtz equation

$$(\Delta + k^2)\psi(\mathbf{r}) = 0 \tag{7}$$

where momentum k [1] is related to the energy E by $k^2 = 2\mu E$.

Extending this analysis to a finite volume $V = L \times L \times L$ with periodic boundary conditions, where the wave function and the potential satisfy

$$\psi(\mathbf{r} + \mathbf{n}L) = \psi(\mathbf{r}) \quad \text{for all} \quad \mathbf{n} \in \mathbb{Z}^3 \tag{8}$$

[1] k is interacting notation to the momentum $|\mathbf{p}_i|$ in the non-interacting case.

$$V_L(\mathbf{r}) = \sum_{\mathbf{n}\in\mathbb{Z}^3} V(\mathbf{r} + \mathbf{n}L) \tag{9}$$

This 3-dimensional Euclidean space with periodic boundary conditions implies that the wave function $\psi(\mathbf{r})$ is on a 3-dimensional torus.

Spherical harmonics and radial wave function solution Suppose the system has solutions $\psi(\mathbf{r})$ to the Schrödinger equation, which can be expanded in spherical harmonics

$$\psi(\mathbf{r}) = \sum_{l=0}^{\infty} \sum_{m=-l}^{l} \psi_{lm}(r) Y_{lm}(\theta, \varphi) \tag{10}$$

where $\mathbf{r}$ is expressed in spherical coordinate

$$\mathbf{r} = r(\sin\theta\cos\varphi, \sin\theta\sin\varphi, \cos\theta) \tag{11}$$

and $Y_{lm}(\theta, \varphi)$ is the spherical harmonics. The solid angles θ and φ are the polar and azimuthal angles, respectively. The radial wave functions $\psi_{lm}(r)$ satisfy the radial differential equation, which have the solutions

$$\psi_{lm}(r) = c_{lm} \left[a_l j_l(kr) + b_l n_l(kr)\right] \tag{12}$$

with proper constants c_{lm}, a_l, b_l and spherical Bessel functions of the first kind $j_l(kr)$ and of the second kind, known as Neumann functions, $n_l(kr)$. The term kr is the product of the magnitude of the momentum k and the magnitude of the relative position r [7]

Green function solution The Helmholtz equation in Eq. 7 is valid in the "exterior region"

$$\Omega = \{\mathbf{r} \in \mathbb{R}^3 | |\mathbf{r}| > R\} \quad \text{for all} \quad \mathbf{n} \in \mathbb{Z}^3 \tag{13}$$

The Helmholtz equation can be solved with a delta function source:

$$(\Delta + k^2)\psi(\mathbf{r}) = -\sum_{\mathbf{n}\in\mathbb{Z}^3} \delta^3(\mathbf{r} + \mathbf{n}L) \tag{14}$$

This admits a general singular periodic solution known as the Green's function $G(\mathbf{r}; k^2)$ [7, 4]. The Green's function is expanded using spherical harmonics:

$$G(\mathbf{r}; k^2) = \sum_{l=0}^{\infty} \sum_{m=-l}^{l} v_{lm} G_{lm}(\mathbf{r}; k^2) \tag{15}$$

where the coefficients v_{lm} are determined by the boundary conditions [4]. The $G_{lm}(\mathbf{r}; k^2)$ is defined as

$$G_{lm}(\mathbf{r}; k^2) = \mathcal{Y}_{lm}(\Delta) G(\mathbf{r}, k^2) \tag{16}$$

using the spherical harmonics relation

$$\mathcal{Y}_{lm}(\Delta) = r^l Y_{lm}(\theta, \varphi) \tag{17}$$

where the angular momentum quantum number $l = 0, 1, 2, ...$ and the magnetic quantum number $m = -l, -l+1, ..., l-1, l$. The Laplacian operator Δ is defined as

$$\Delta = \frac{1}{r}\frac{\partial^2}{\partial r^2} r - \frac{l(l+1)}{r^2} + \frac{1}{r^2}\Delta_{\theta,\varphi} \tag{18}$$

where $\Delta_{\theta,\varphi}$ is the angular part of the Laplacian operator.

The specific form of the Green's function $G_{lm}(\mathbf{r}; k^2)$ involves spherical Bessel functions n_l and Neumann functions j_l, and is given by:

$$G_{lm}(\mathbf{r}; k^2) = \frac{(-1)^l k^{l+1}}{4\pi} \left\{ n_l(kr) Y_{lm}(\theta, \varphi) + \sum_{l'=0}^{\infty} \sum_{m'=-l}^{l} M_{lm,l'm'}(q) j_{l'}(kr) Y_{l'm'}(\theta, \varphi) \right\} \tag{19}$$

where the coefficient $M_{lm,l'm'}(q)$ is

$$M_{lm,l'm'}(q) = \frac{(-1)^l}{\pi^{3/2}} \sum_{j=|l-l'|}^{l+l'} \sum_{s=-j}^{j} \frac{i^j}{q^{j+1}} \mathcal{Z}_{js}(1; q^2) C_{lm,js,l'm'} \tag{20}$$

with the dimensionless momentum quantity q

$$q = \frac{kL}{2\pi} \tag{21}$$

The tensor $C_{lm,js,l'm'}$ can be written in terms of Wigner 3j-symbols

$$C_{lm,js,l'm'} = (-1)^{m'} i^{l-j+l'} \sqrt{(2l+1)(2j+1)(2l'+1)} \begin{pmatrix} l & j & l' \\ m & s & -m' \end{pmatrix} \begin{pmatrix} l & j & l' \\ 0 & 0 & 0 \end{pmatrix} \tag{22}$$

The Zeta function $\mathcal{Z}_{lm}(s; q^2)$ is defined as

$$\mathcal{Z}_{lm}(s; q^2) = \sum_{\mathbf{n} \in \mathbb{Z}^3} \frac{\mathcal{Y}_{lm}(\mathbf{n})}{(\mathbf{n}^2 - q^2)^s} \tag{23}$$

where the spherical harmonics $\mathcal{Y}_{lm}(\mathbf{r})$ for a point is

$$\mathcal{Y}_{lm}(\mathbf{r}) = |\mathbf{r}|^l Y_{lm}(\theta, \varphi) \tag{24}$$

. This is the product of spherical harmonics of degree l and a radial component $|\mathbf{r}|^l$, known as solid harmonics [8].

2.1.3 Phase information

The physics is straightforward in the non-interacting case. However, in the interacting case, the potential generated by the interaction between the two particles, for example, strong forces coupled by gluons in QCD between quarks, complicates the system. The Lattice QCD method succeeds in simulating the interaction in such a scenario and providing the energy spectrum of the system, where only discrete energy levels are permissible. This information yields phase shifts δ_l in the partial waves, which are crucial for understanding the resonance and scattering phenomena.

In the general wave function solution (Eq. 10), the phase shift δ_l in the infinite volume of three dimensions is defined through the ratio of the out-going and in-going wave functions

$$e^{2i\delta_l(k)} = \frac{a_l(k) + ib_l(k)}{a_l(k) - ib_l(k)} \tag{25}$$

with the coefficients $a_l(k)$ and $b_l(k)$ in Eq. 12 [9].

To determine δ_l, we connect the two wave functions expressed in spherical harmonics expression (Eq. 10) with the Green function (Eq. 15). By equating the spherical harmonics terms $Y_{lm}n_l(kr)$ and $Y_{lm}j_{l\prime}(kr)$, the coefficients are related [10]

$$c_{lm}b_l = v_{lm}\frac{(-1)^l(k)^{l+1}}{4\pi} \tag{26}$$

$$c_{lm}a_l = \sum_{l',m'} v_{l'm'}\frac{(-1)^{l'}(k)^{l'+1}}{4\pi}M_{l'm',lm}(q) \tag{27}$$

Expressing v_{lm} in the first one and substituting it into the second one gives

$$\sum_{l',m'} c_{l'm'}\left[b_l M_{l'm',lm}(q) - a_l\delta_{ll'}\delta_{mm'}\right] = 0 \tag{28}$$

This equation can be cast into a matrix form and it has a non-trivial solution only when the determinant of the matrix is zero.

$$\det(BM - A) = 0 \tag{29}$$

where the matrix M is $M_{l'm',lm}(q)$, $A_{l'm',lm} = a_l\delta_{l'l}\delta_{m'm}$, and $B_{l'm',lm} = b_l\delta_{l'l}\delta_{m'm}$. Utilizing the phase shift relation (Eq. 25), that is $e^{2i\delta} = \frac{A+iB}{A-iB}$ in matrix form, we can show that

$$\det\left[e^{2i\delta}(M - i) - (M + i)\right] = 0 \tag{30}$$

is a valid representation via

$$\det\left[e^{2i\delta_l}(M-i)-(M+i)\right] \tag{31}$$
$$=\det\left[\frac{A+iB}{A-iB}(M-i)-(M+i)\right] \tag{32}$$
$$=\det\left[\frac{(A+iB)(M-i)-(A-iB)(M+i)}{A-iB}\right] \tag{33}$$
$$=\det\left[\frac{AM+iBM-Ai+B-AM-Ai+iBM-B}{A-iB}\right] \tag{34}$$
$$=\det\left[\frac{-2Ai+2iBM}{A-iB}\right] \qquad =0 \tag{35}$$

$\det(A-iB)$ is non-zero as the phase shift $\delta_l(k)$ (Eq. 25) is a well defined real analytic function [4]. By dividing $\det(A-iB)$ and removing the factor of $-2i$ in Eq. 35, we prove that Eq. 30 is equivalent to the quantization condition of the phase shift in Eq. 29.

Another representation using the diagonal matrices $\cos\delta = \cos\delta_l\delta_{ll'}\delta_{mm'}$ and $\sin\delta = \sin\delta_l\delta_{ll'}\delta_{mm'}$ by diagonalizing the matrix is [11]

$$\det(\cos\delta - \sin\delta\cdot i^{-l_1}M_{l_1m_1,l_2m_2}i^{l_2}) = 0 \tag{36}$$

This quantization condition is pivotal in determining the phase shift from the matrix M, which depends on the dimensionless momentum vector q. Recall that this vector q is associated with the energy spectrum in the lattice QCD simulation of the system. As a result, we can extract the phase shift δ_l from the quantization condition based on the energy levels of the system.

Assuming the higher order partial waves vanish, i.e. $M_{l'm',lm} = 0$, or equivalently, the $\delta_l = 0$, for $l' > l_{max}$. This truncates the quantization condition to:

$$\det(BM-A)|_{l_1,l_2\leq l_{max}} = 0 \tag{37}$$

resulting in a finite matrix equation that can be solved numerically to extract the phase shifts δ_l.

For a $l_{max} = 1$, where the matrix M is a 4×4 matrix, the phase shift is the same for S-wave ($l=1$) and P-wave ($l=1$), that is

$$\tan\delta_0(k) = \tan\delta_1(k) = \frac{\pi^{\frac{3}{2}}q}{\mathcal{Z}_{00}(1,q^2)} \tag{38}$$

with q defined in Eq. 21 [10, 12].

2.1.4 Mapping between infinite volume and finite volume

In an infinite volume, the energy spectrum is continuous due to the unbounded nature of the system. Consequently, determining the phase shift δ_l becomes impractical since wave functions extend indefinitely. In contrast, in a finite volume, the energy levels are discrete, allowing for the extraction of the phase shift δ_l from the wave functions, given that the asymptotic behavior is regularized at large time-distances [13].

For small interaction ranges typical in QCD, the finite-range interactions governing the scattering amplitudes of two hadrons in both infinite and finite volumes remain analogous. But in the finite volume case, there exists a shift in the energy levels compared to the free system. Therefore, given that the range of interactions is small compared with the extent of the volume, the phase shift δ_l in the finite volume and in the infinite volume must be ultimately related [14].

It is worth pointing out that although the energy levels correspond to a finite volume $V = L^3$, the phase shift $\delta(k)$ is fundamentally defined in the infinite-volume phase shift. This connection assumes the volume $V = L^3$ exceeds the spatial extent of the two-pion interaction region [4]. The phase shifts for $\pi\pi$ scattering are reliable for pion mass above 200MeV and lattice size $L \geq 2$fm because the convergence of the field theory is guaranteed [15].

2.1.5 Physics for convergence

The Luscher Zeta function $\mathcal{Z}_{lm}(s; q^2)$ encounters an ultraviolet divergence, where the integral diverges due to the contributions from objects with unbounded energy. For instance, the pion-pion scattering may have their interaction in an arbitrary number of loops, as depicted in Fig. 1. This results in an infinite product of the scattering matrices, which denotes the scattering process between initial and final states. As such, an infinite loop causes the unbounded energy situation [11].

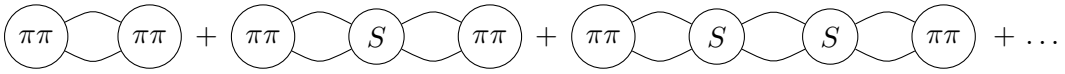

Figure 1: Contributions to correlation function in the pion-pion scattering process. $\pi\pi$ denotes an initial or final state of two pions. S is the scattering matrix.

The divergence in such infinite products requires a physical meaning. The solution comes with the regularization, usually by way of the Riemann Zeta function [16].

$$\zeta(s) = \sum_{n=1}^{\infty} \frac{1}{n^s} \tag{39}$$

Named after Riemann Zeta, the $\mathcal{Z}_{lm}$ function is a generalization of this on Lattice QCD.

The $\mathcal{Z}_{lm}(s; q^2)$ converges for $s > \frac{3}{2}$ given $\mathbf{n}^2 \neq q^2$. Whereas we are interested in $s = 1$ case, the $\mathcal{Z}_{lm}(s; q^2)$ is finite for $l \geq 1$ and diverges for $l = 0$ case. However, the divergence

of $l = m = 0$ in $s = 1$ for the Zeta function also appears in the infinite volume case. While the phase shift relates the finite volume to the infinite volume, this divergence is not physical because it cancels out in two cases. Therefore, we can get rid of it by the analytic continuation from $s > 3/2$ to $s = 1$ (will be shown in 2.2.1) [10].

2.2 Evaluation of Luscher Zeta function

In this section, we will explore three distinct approaches—Luscher's, Savage's, and Leskovec's methods—to derive an alternative expression for the Zeta function that is well-suited for numerical evaluation. These methods focus on scenarios involving two equal-mass particles in a stationary frame.

2.2.1 Luscher's method

The Zeta function $\mathcal{Z}_{lm}(s; q^2)$ is first separated into two parts with cutoff Λ such that $\Lambda^2 > \Re q^2$. The singular case $n^2 = q^2$ can be excluded [4].

$$\mathcal{Z}_{lm}(s; q^2) = \sum_{|\mathbf{n}|<\Lambda} \frac{1}{(\mathbf{n}^2 - q^2)^s} \mathcal{Y}_{lm}(\mathbf{n}) + \sum_{|\mathbf{n}|>\Lambda} \frac{1}{(\mathbf{n}^2 - q^2)^s} \mathcal{Y}_{lm}(\mathbf{n}) \tag{40}$$

The first term in Eq. 40 is finite and can be evaluated directly. The second term is divergent and requires simplification for numerical evaluation.

Gamma functions We first introduce the gamma functions

$$\Gamma(s) = \int_0^\infty t^{s-1} e^{-t} dt \tag{41}$$

$$\Gamma(s, c) = \int_c^\infty t^{s-1} e^{-t} dt \tag{42}$$

$$\gamma(s, c) = \int_0^c t^{s-1} e^{-t} dt \tag{43}$$

The $\Gamma(s, c)$ and $\gamma(s, c)$ are upper and lower incomplete gamma functions. For $c > 0$ and $\Re(s) > 0$, the following relation holds

$$\frac{1}{\Gamma(s)} \int_0^\infty t^{s-1} e^{-ct} dt = \frac{1}{\Gamma(s) c^{s-1}} \int_0^\infty (ct)^{s-1} e^{-ct} \frac{d(ct)}{c} \tag{44}$$

$$= \frac{1}{\Gamma(s) c^s} \int_0^\infty (ct)^{s-1} e^{-ct} d(ct) \tag{45}$$

$$= \frac{1}{\Gamma(s) c^s} \Gamma(s) \tag{46}$$

$$= \frac{1}{c^s} \tag{47}$$

Let $c = \mathbf{n}^2 - q^2$, the second term in Eq. 40 can be written as

$$\sum_{|\mathbf{n}|>\Lambda} \frac{1}{(\mathbf{n}^2 - q^2)^s} \mathcal{Y}_{lm}(\mathbf{n}) = \sum_{|\mathbf{n}|>\Lambda} \frac{1}{\Gamma(s)} \mathcal{Y}_{lm}(\mathbf{n}) \int_0^\infty t^{s-1} e^{-(\mathbf{n}^2 - q^2)t} dt \tag{48}$$

Heat kernel We now use the heat kernel, which has a time-varying Gaussian function, originating from the heat equation [17]. The heat kernel $\mathcal{K}(t, \mathbf{r})$ is defined as

$$\mathcal{K}(t, \mathbf{r}) = \frac{1}{(2\pi)^3} \sum_{\mathbf{n} \in \mathbb{Z}^3} e^{i\mathbf{n}\cdot\mathbf{r} - t\mathbf{n}^2} \tag{49}$$

Poisson summation formula The Poisson summation formula is used to find an alternative representation of the heat kernel. The Poisson summation formula in 1 dimension [18] is given by

$$\sum_{n=-\infty}^{n=+\infty} f(n) = \sum_{\xi=-\infty}^{\xi=+\infty} \hat{f}(\xi) \tag{50}$$

where $\hat{f}(\xi)$ is the Fourier transform of $f(n)$,

$$\hat{f}(\xi) = \int_{-\infty}^{+\infty} e^{-2\pi i n \xi} f(n) dn \tag{51}$$

In 3 dimensions, the Poisson summation formula is

$$\sum_{\mathbf{n} \in \mathbb{Z}^3} f(\mathbf{n}) = \sum_{\boldsymbol{\xi} \in \mathbb{Z}^3} \hat{f}(\boldsymbol{\xi}) \tag{52}$$

where $\hat{f}(\boldsymbol{\xi})$ is the Fourier transform of $f(\mathbf{n})$ [2]

$$\hat{f}(\boldsymbol{\xi}) = \int_{-\infty}^{+\infty} e^{-2\pi i \mathbf{n}\cdot\boldsymbol{\xi}} f(\mathbf{n}) d^3\mathbf{n} \tag{53}$$

Gaussian integral One of the Gaussian integrals used here is

$$\int_{-\infty}^{+\infty} e^{-ax^2 + bx} dx = \sqrt{\frac{\pi}{a}} e^{\frac{b^2}{4a}} \tag{54}$$

[2] The vectors $\mathbf{n}, \mathbf{r}, \boldsymbol{\xi}$ can be written as $\mathbf{n} = (n_1, n_2, n_3)$, $\mathbf{r} = (r_1, r_2, r_3)$, $\boldsymbol{\xi} = (\xi_1, \xi_2, \xi_3)$.

The summation part in heat kernel (Eq. 49) can be written as

$$\sum_{\mathbf{n}\in\mathbb{Z}^3} e^{i\mathbf{n}\cdot\mathbf{r}-t\mathbf{n}^2} = \sum_{\boldsymbol{\xi}\in\mathbb{Z}^3} \int_{-\infty}^{+\infty} e^{i\mathbf{n}\cdot\mathbf{r}-t\mathbf{n}^2} e^{-2\pi i\mathbf{n}\cdot\boldsymbol{\xi}} d\mathbf{n}$$

[Poisson Summation] (55)

$$= \sum_{\boldsymbol{\xi}\in\mathbb{Z}^3} \int_{-\infty}^{+\infty} e^{i\mathbf{n}\cdot(\mathbf{r}-2\pi\boldsymbol{\xi})-t\mathbf{n}^2} d\mathbf{n} \tag{56}$$

$$= \prod_{i=1}^{i=3} \sum_{\xi_i=-\infty}^{\xi_i=+\infty} \int_{n_i=-\infty}^{n_i=+\infty} e^{in_i(r_i-2\pi\xi_i)-tn_i^2} dn_i$$

[Split into three terms, one for each component] (57)

$$= \prod_{i=1}^{i=3} \sum_{\xi_i=-\infty}^{\xi_i=+\infty} \sqrt{\frac{\pi}{t}} e^{-\frac{(r_i-2\pi\xi_i)^2}{4t}}$$

[Gaussian Integral] (58)

$$= \left(\sqrt{\frac{\pi}{t}}\right)^3 \sum_{\boldsymbol{\xi}\in\mathbb{Z}^3} e^{-\frac{(\mathbf{r}-2\pi\boldsymbol{\xi})^2}{4t}}$$

[Rewrite to vector form] (59)

We can now change the dummy variable $\boldsymbol{\xi} \to \mathbf{n}$ in Eq. 59, and substitute it back into Eq. 49 to get an alternative expression for the heat kernel.

$$\mathcal{K}(t,\mathbf{r}) = \frac{1}{(2\pi)^3} \left(\sqrt{\frac{\pi}{t}}\right)^3 \sum_{\mathbf{n}\in\mathbb{Z}^3} e^{-\frac{(\mathbf{r}-2\pi\mathbf{n})^2}{4t}} \tag{60}$$

$$= \frac{1}{(4\pi t)^{\frac{3}{2}}} \sum_{\mathbf{n}\in\mathbb{Z}^3} e^{-\frac{(\mathbf{r}-2\pi\mathbf{n})^2}{4t}} \tag{61}$$

Using

$$\sum_{|\mathbf{n}|>\Lambda} = \sum_{\mathbf{n}\in\mathbb{Z}^3} - \sum_{|\mathbf{n}|<\Lambda} \tag{62}$$

the truncated heat kernel is

$$\mathcal{K}^\Lambda(t,\mathbf{r}) = \frac{1}{(2\pi)^3} \sum_{|\mathbf{n}|>\Lambda} e^{i\mathbf{n}\cdot\mathbf{r}-t\mathbf{n}^2} \tag{63}$$

$$= \mathcal{K}(t,\mathbf{r}) - \frac{1}{(2\pi)^3} \sum_{|\mathbf{n}|<\Lambda} e^{i\mathbf{n}\cdot\mathbf{r}-t\mathbf{n}^2} \tag{64}$$

The truncated heat kernel evaluated at $\mathbf{r} = \vec{0}$ is

$$\begin{aligned}
&\mathcal{K}^{\Lambda}(t,\vec{0}) \\
&= \mathcal{K}^{\Lambda}_{(large)}(t,\vec{0}) = \frac{1}{(2\pi)^3}\sum_{|\mathbf{n}|>\Lambda} e^{-t\mathbf{n}^2} \qquad \text{evaluation for} \quad t \geq 1 \qquad (65)\\
&= \mathcal{K}^{\Lambda}_{(small)}(t,\vec{0}) = \frac{1}{(4\pi t)^{\frac{3}{2}}}\sum_{|\mathbf{n}|>\Lambda} e^{-\frac{\pi^2\mathbf{n}^2}{t}} \qquad \text{evaluation for} \quad t < 1 \qquad (66)
\end{aligned}$$

Both equations are equivalent, but their usage depends on the value of t to achieve faster convergence.

$\mathcal{Z}_{00}$ case By using the Gamma integrals, Poisson summation formula and the truncated heat kernels, the Zeta function $\mathcal{Z}_{00}(s;q^2)$ can be written as

$$\begin{aligned}
\mathcal{Z}_{00}(s;q^2) &= \sum_{|\mathbf{n}|<\Lambda}\frac{1}{(\mathbf{n}^2-q^2)^s}\mathcal{Y}_{00}(\mathbf{n}) + \sum_{|\mathbf{n}|>\Lambda}\frac{1}{(\mathbf{n}^2-q^2)^s}\mathcal{Y}_{00}(\mathbf{n}) && (67)\\
&= \frac{1}{\sqrt{4\pi}}\sum_{|\mathbf{n}|<\Lambda}\frac{1}{(\mathbf{n}^2-q^2)^s} + \frac{1}{\sqrt{4\pi}}\sum_{|\mathbf{n}|>\Lambda}\frac{1}{(\mathbf{n}^2-q^2)^s} && (68)\\
&= \frac{1}{\sqrt{4\pi}}\sum_{|\mathbf{n}|<\Lambda}\frac{1}{(\mathbf{n}^2-q^2)^s} + \frac{1}{\sqrt{4\pi}}\sum_{|\mathbf{n}|>\Lambda}\frac{1}{\Gamma(s)}\int_0^{\infty} t^{s-1}e^{-(\mathbf{n}^2-q^2)t}dt && (69)\\
&= \frac{1}{\sqrt{4\pi}}\sum_{|\mathbf{n}|<\Lambda}\frac{1}{(\mathbf{n}^2-q^2)^s} + \frac{1}{\sqrt{4\pi}\Gamma(s)}\int_0^{\infty} t^{s-1}e^{q^2t}\sum_{|\mathbf{n}|>\Lambda}e^{-t\mathbf{n}^2}dt && (70)\\
&= \frac{1}{\sqrt{4\pi}}\sum_{|\mathbf{n}|<\Lambda}\frac{1}{(\mathbf{n}^2-q^2)^s} + \frac{(2\pi)^3}{\sqrt{4\pi}\Gamma(s)}\int_0^{\infty} t^{s-1}e^{q^2t}\mathcal{K}^{\Lambda}(t,\vec{0})dt && (71)
\end{aligned}$$

Since the heat kernel has two representations, in which the convergence differs for t. The integral from 0 to ∞ can be split into two parts, from 0 to 1 and from 1 to ∞,

$$\begin{aligned}
\mathcal{Z}_{00}(s;q^2) &= \frac{1}{\sqrt{4\pi}}\sum_{|\mathbf{n}|<\Lambda}\frac{1}{(\mathbf{n}^2-q^2)^s} && (72)\\
&+ \frac{(2\pi)^3}{\sqrt{4\pi}\Gamma(s)}\left\{\int_0^1 t^{s-1}e^{q^2t}\mathcal{K}^{\Lambda}(t,\vec{0})dt + \int_1^{\infty} t^{s-1}e^{q^2t}\mathcal{K}^{\Lambda}(t,\vec{0})dt\right\} && (73)
\end{aligned}$$

Recall the cutoff Λ is chosen such that $\Lambda^2 > \Re q^2$. As $\Lambda^2 \to \Re q^2$ and $t \to 0$, for $\mathcal{Z}_{00}(s;q^2)$ case,

$$\begin{aligned}
e^{q^2t}\mathcal{K}^{\Lambda}(t,\vec{0}) &= e^{q^2t}\frac{1}{(4\pi t)^{\frac{3}{2}}}\sum_{|\mathbf{n}|>\Lambda} e^{-\frac{\mathbf{n}^2}{4t}} && (74)\\
&= \frac{1}{(4\pi t)^{\frac{3}{2}}}\sum_{|\mathbf{n}|>\Lambda} e^{q^2t-\frac{\mathbf{n}^2}{4t}} && (75)
\end{aligned}$$

It is possible to have the exponential term $e^{q^2 t - \frac{\mathbf{n}^2}{4t}}$ to be 1, in which the integral is divergent at $t \to 0$, leading to the asymptotic behavior. Therefore,

$$e^{q^2 t}\mathcal{K}^{\Lambda}(t,\vec{0}) = \frac{1}{(4\pi t)^{\frac{3}{2}}} + \mathcal{O}(t^{-\frac{1}{2}}) \tag{76}$$

In the integral from 0 to 1, the asymptotic behaviour part is

$$\begin{aligned}\lim_{\epsilon\to 0^+}\int_{\epsilon}^{1} t^{s-1}\frac{1}{t^{\frac{3}{2}}}dt &= \lim_{\epsilon\to 0^+}\int_{\epsilon}^{1} t^{s-1-\frac{3}{2}}dt \\ &= \lim_{\epsilon\to 0^+}\left[\frac{t^{s-\frac{3}{2}}}{s-\frac{3}{2}}\right]_{\epsilon}^{1}\end{aligned} \tag{77}$$

The limit can be evaluated for $\Re s > \frac{3}{2}$,

$$\lim_{\epsilon\to 0^+}\int_{\epsilon}^{1} t^{s-\frac{3}{2}}dt = \frac{1}{s-\frac{3}{2}} \tag{78}$$

We analytic continue it to $s = 1$

$$\int_0^1 t^{s-\frac{5}{2}}dt \overset{\Re s>\frac{3}{2}}{=\!=} \frac{1}{s-\frac{3}{2}} \overset{s=1}{\longrightarrow} -2 \tag{79}$$

Following this observation, by subtracting off the leading divergence, the Zeta function $\mathcal{Z}_{00}(s;q^2)$ in Eq. 73 can be written as

$$\begin{aligned}\mathcal{Z}_{00}(s;q^2) = &\frac{1}{\sqrt{4\pi}}\sum_{|\mathbf{n}|<\Lambda}\frac{1}{(\mathbf{n}^2-q^2)^s} \\ &+ \frac{(2\pi)^3}{\sqrt{4\pi}\Gamma(s)}\left\{\frac{1}{(4\pi)^{\frac{3}{2}}}\cdot\frac{1}{s-\frac{3}{2}} + \int_0^1 t^{s-1}\left[e^{q^2 t}\mathcal{K}^{\Lambda}(t,\vec{0}) - \frac{1}{(4\pi t)^{\frac{3}{2}}}\right]dt\right. \\ &\left. + \int_1^{\infty} t^{s-1}e^{q^2 t}\mathcal{K}^{\Lambda}(t,\vec{0})dt\right\}\end{aligned} \tag{80}$$

This is valid for all l, m and s in the real half plane $\Re s > \frac{1}{2}$ and coincides with Eq. 71 for $\Re s > \frac{1}{2}$. Eq. 80 is then the unique analytic continuation of Eq. 71 from the real half plane $\Re s > \frac{3}{2}$ to $\Re s > \frac{1}{2}$.

The Zeta function in Eq 80 is sufficient to analyze numerically, with the plugin of the heat kernel for $t < 1$ with Eq. 66 and $t > 1$ with Eq. 65. For $s = 1$ case, the Gamma

function $\Gamma(s=1)=1$, and the Zeta function $\mathcal{Z}_{00}(1;q^2)$ can be written as

$$\begin{aligned}\mathcal{Z}_{00}(1;q^2) = &\sum_{|\mathbf{n}|<\Lambda} \frac{1}{\mathbf{n}^2-q^2}\frac{1}{\sqrt{4\pi}} \\ &+ (2\pi)^3\left\{\frac{-2}{(4\pi)^2} + \int_0^1 \frac{1}{\sqrt{4\pi}}\left[e^{q^2t}\mathcal{K}^{\Lambda}(t,\vec{0}) - \frac{1}{(4\pi t)^{\frac{3}{2}}}\right]dt \right. \\ &\left. + \int_1^{\infty}\frac{1}{\sqrt{4\pi}}e^{q^2t}\mathcal{K}^{\Lambda}(t,\vec{0})dt\right\} \end{aligned} \tag{81}$$

Expanding in terms of the small and large kernels gives

$$\begin{aligned}\mathcal{Z}_{00}(1;q^2) = &\sum_{|\mathbf{n}|<\Lambda} \frac{1}{\mathbf{n}^2-q^2}\frac{1}{\sqrt{4\pi}} \\ &+ (2\pi)^3\left\{\frac{-2}{(4\pi)^2} + \int_0^1 \frac{1}{\sqrt{4\pi}}\left[e^{q^2t}\left(\mathcal{K}(t,\vec{0}) - \mathcal{K}^{<\Lambda}_{(large)}(t,\vec{0})\right) - \frac{1}{(4\pi t)^{\frac{3}{2}}}\right]dt \right. \\ &\left. + \int_1^{\infty}\frac{1}{\sqrt{4\pi}}e^{q^2t}\mathcal{K}^{\Lambda}_{(large)}(t,\vec{0})dt\right\} \end{aligned} \tag{82}$$

In the integral for $t\in(0,1)$, the truncated heat kernel $\mathcal{K}^{\Lambda}(t,\vec{0})$ is the subtraction of the alternative representation of the kernel (Eq. 61) to the large kernel for $|\mathbf{n}<\Lambda|$ (Eq. 65). This subtraction follows the truncated heat kernel definition in Eq. 62.

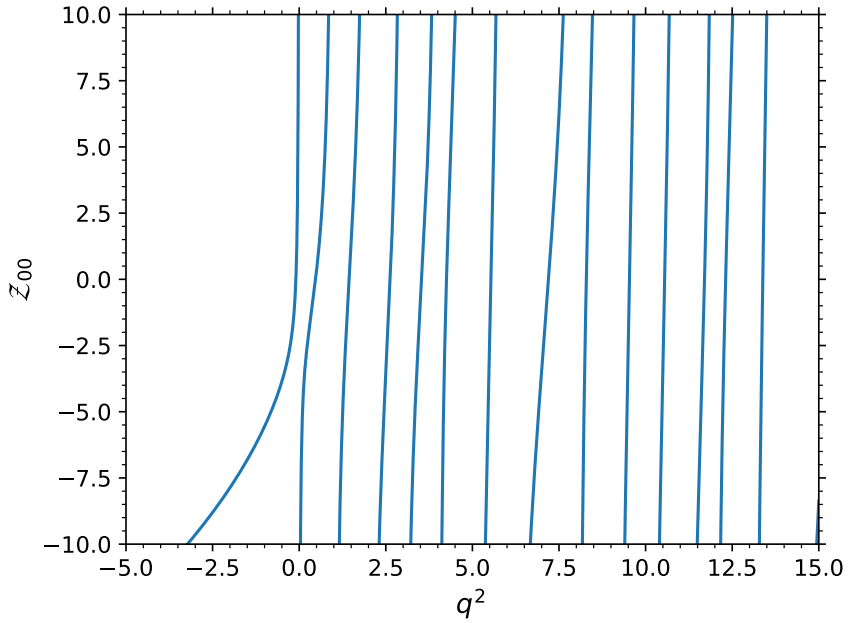

Figure 2: Plot of the Zeta function $\mathcal{Z}_{00}(1;q^2)$

Figure 2 shows the plot of the Zeta function $\mathcal{Z}_{00}(1;q^2)$ for $q^2 \in [-5,15]$. The asymptotic behavior of the Zeta function is observed at $\mathbf{n}^2 = q^2$. For example $q^2 = 0,1,2,3,...$, when $\mathbf{n} = (0,0,0)^T, (1,0,0)^T, (1,1,0)^T, (1,1,1)^T, ...$ respectively.

$\mathcal{Z}_{lm}$ case In the situation where $l \neq 0$, the Zeta function $\mathcal{Z}_{lm}(s;q^2)$ is finite for all s and can be evaluated directly. Following the same procedure as in the $\mathcal{Z}_{00}$ case, the truncated heat kernels are now coupled with the term $\mathcal{Y}_{lm}(\mathbf{n})$.

$$\mathcal{K}^{\Lambda}_{lm}(t,\vec{0}) = \mathcal{K}^{\Lambda}_{lm;(large)}(t,\vec{0}) \qquad = \frac{1}{(2\pi)^3}\sum_{|\mathbf{n}|>\Lambda} \mathcal{Y}_{lm}(\mathbf{n}) e^{-t\mathbf{n}^2} \quad \text{for} \quad t \geq 1 \tag{83}$$

To derive the alternative expression for the heat kernel, we would expand the spherical harmonics relation in Eq. 24.

$$\mathcal{K}_{lm;(large)}(t,\vec{0}) = \frac{1}{(2\pi)^3}\sum_{|\mathbf{n}|\in\mathcal{Z}^3} \mathcal{Y}_{lm}(\mathbf{n}) e^{-t\mathbf{n}^2} \tag{84}$$

$$= \frac{1}{(2\pi)^3}\sum_{|\mathbf{n}|\in\mathcal{Z}^3} |\mathbf{n}|^l Y_{lm}(\theta,\varphi) e^{-t\mathbf{n}^2} \tag{85}$$

To apply the Poisson summation formula (Eq. 52), the Fourier transform $\hat{f}(\boldsymbol{\xi})$ of $f(\mathbf{n})$ is

$$\hat{f}(\boldsymbol{\xi}) = \int_{-\infty}^{+\infty} e^{-2\pi i \mathbf{n}\cdot\boldsymbol{\xi}} f(\mathbf{n}) d^3\mathbf{n} \tag{86}$$

$$= \int_{-\infty}^{+\infty} e^{-2\pi i \mathbf{n}\cdot\boldsymbol{\xi}} |\mathbf{n}|^l Y_{lm}(\theta,\varphi) e^{-t\mathbf{n}^2} d^3\mathbf{n} \tag{87}$$

The integral can be written in spherical coordinates (Eq. 11).

$$\hat{f}(\boldsymbol{\xi}) = \int_0^{2\pi} d\varphi \int_0^{\pi} d\theta \int_0^{\infty} dr r^2 \sin\theta e^{-2\pi i \mathbf{r}\cdot\boldsymbol{\xi}} r^l Y_{lm}(\theta,\varphi) e^{-tr^2} \tag{88}$$

$$= \int_0^{\infty} dr r^2 r^l e^{-tr^2} \int_0^{\pi} d\theta \sin\theta \int_0^{2\pi} d\varphi e^{-i\mathbf{k}\cdot\mathbf{r}} Y_{lm}(\theta,\varphi) \tag{89}$$

with $\mathbf{k} \equiv 2\pi\boldsymbol{\xi}$. Using the plain wave expansion of $e^{i\mathbf{k}\cdot\mathbf{r}}$, also known as the Rayleigh expansion [19]

$$e^{-i\mathbf{k}\cdot\mathbf{r}} = 4\pi \sum_{l=0}^{\infty}\sum_{m=-l}^{l} (-i)^l j_l(kr) Y^*_{lm}(\theta_r,\varphi_r) Y_{lm}(\theta_k,\varphi_k) \tag{90}$$

where $j_l(kr)$ is the spherical Bessel function of the first kind as used in Eq. 12 and θ_r, φ_r are the polar and azimuthal angles of $\mathbf{r}$. Similar for θ_k, φ_k.

Using the orthogonality of the spherical harmonics, where

$$\int_0^{\pi} d\theta \sin\theta \int_0^{2\pi} d\varphi Y_{lm}(\theta,\varphi) Y^*_{l'm'}(\theta,\varphi) = \delta_{ll'}\delta_{mm'} \tag{91}$$

the Fourier transform $\hat{f}(\boldsymbol{\xi})$ simplifies to

$$\hat{f}(\boldsymbol{\xi}) = 4\pi(-i)^l Y_{lm}(\theta_k,\varphi_k) \int_0^{\infty} dr r^{l+2} e^{-tr^2} j_l(kr) \tag{92}$$

The integral

$$\int_0^{\infty} dr r^{l+2} e^{-tr^2} j_l(kr) \tag{93}$$

can be simplified with the known integral of the Bessel function [20]

$$\int_0^{\infty} x^{\nu+1} e^{-\alpha x^2} J_\nu(\beta x)\, dx = \frac{\beta^\nu}{(2\alpha)^{\nu+1}} \exp\left(-\frac{\beta^2}{4\alpha}\right) \quad \text{for} \quad \Re\alpha > 0, \Re\nu > -1 \tag{94}$$

where $J_\nu(\beta x)$ is the regular Bessel function. The linkage between the regular Bessel function and the spherical Bessel function is

$$j_l(kr) = \sqrt{\frac{\pi}{2kr}} J_{l+1/2}(kr) \tag{95}$$

The integral in Eq. 93 is then

$$\begin{aligned}
\int_0^{\infty} dr r^{l+2} e^{-tr^2} j_l(kr) &= \int_0^{\infty} dr r^{l+2} e^{-tr^2} \sqrt{\frac{\pi}{2kr}} J_{l+1/2}(kr) && (96)\\
&= \sqrt{\frac{\pi}{2k}} \int_0^{\infty} dr r^{l+\frac{3}{2}} e^{-tr^2} J_{l+1/2}(kr) && (97)\\
&= \sqrt{\frac{\pi}{2k}} \frac{k^{l+1/2}}{(2t)^{l+3/2}} \exp\left(-\frac{k^2}{4t}\right) && (98)\\
&= \sqrt{\frac{\pi}{2}} \frac{k^{l}}{(2t)^{l+3/2}} \exp\left(-\frac{k^2}{4t}\right) && (99)
\end{aligned}$$

by setting $\alpha = t$, $\nu = l + 1/2$, and $\beta = k$. Substituting Eq. 99 back to Eq. 92, the Fourier transform $\hat{f}(\boldsymbol{\xi})$ is

$$\begin{aligned}
\hat{f}(\boldsymbol{\xi}) &= 4\pi(-i)^l Y_{lm}(\theta_k,\varphi_k) \sqrt{\frac{\pi}{2}} \frac{k^l}{(2t)^{l+3/2}} \exp\left(-\frac{k^2}{4t}\right) && (100)\\
&= (-i)^l Y_{lm}(\theta_k,\varphi_k) \left(\frac{k}{2t}\right)^l \left(\frac{\pi}{t}\right)^{\frac{3}{2}} \exp\left(-\frac{k^2}{4t}\right) && (101)
\end{aligned}$$

Using Eq. 24, we can further simplify by applying

$$\left(\frac{k}{2t}\right)^{l} Y_{lm}(\theta_k, \varphi_k) = \mathcal{Y}_{lm}\left(\frac{\mathbf{k}}{2t}\right) \tag{102}$$

$$= \mathcal{Y}_{lm}\left(\frac{\pi\boldsymbol{\xi}}{t}\right) \tag{103}$$

The Fourier transform $\hat{f}(\boldsymbol{\xi})$ is then

$$\hat{f}(\boldsymbol{\xi}) = (-i)^l \mathcal{Y}_{lm}\left(\frac{\pi\boldsymbol{\xi}}{t}\right)\left(\frac{\pi}{t}\right)^{\frac{3}{2}} \exp\left(-\frac{\pi^2\boldsymbol{\xi}^2}{t}\right) \tag{104}$$

and the Poisson summation formula (Eq. 52) can be applied to the Fourier transform $\hat{f}(\boldsymbol{\xi})$.

$$\sum_{\mathbf{n}\in\mathbb{Z}^3} f(\mathbf{n}) = \sum_{\boldsymbol{\xi}\in\mathbb{Z}^3} \hat{f}(\boldsymbol{\xi}) \tag{105}$$

$$= \sum_{\boldsymbol{\xi}\in\mathbb{Z}^3} (-i)^l \mathcal{Y}_{lm}\left(\frac{\pi\boldsymbol{\xi}}{t}\right)\left(\frac{\pi}{t}\right)^{\frac{3}{2}} \exp\left(-\frac{\pi^2\boldsymbol{\xi}^2}{t}\right) \tag{106}$$

Therefore, the heat kernel $\mathcal{K}_{lm}(t, \vec{0})$ is

$$\mathcal{K}_{lm}(t, \vec{0})$$

$$= \mathcal{K}_{lm;(large)}(t, \vec{0}) = \frac{1}{(2\pi)^3} \sum_{|\mathbf{n}|\in\mathcal{Z}^3} \mathcal{Y}_{lm}(\mathbf{n}) e^{-t\mathbf{n}^2} \qquad \text{for} \quad t \geq 1 \tag{107}$$

$$= \mathcal{K}_{lm;(small)}(t, \vec{0}) = \frac{1}{(2\pi)^3} \sum_{\mathbf{n}\in\mathbb{Z}^3} (-i)^l \mathcal{Y}_{lm}\left(\frac{\pi\mathbf{n}}{t}\right)\left(\frac{\pi}{t}\right)^{\frac{3}{2}} \exp\left(-\frac{\pi^2\mathbf{n}^2}{t}\right) \quad \text{for} \quad t < 1 \tag{108}$$

With the truncated heat kernel definition in Eq. 62 and following a similar procedure as in the $\mathcal{Z}_{00}$ case (Sec 2.2.1), the Zeta function $\mathcal{Z}_{l\neq 0,m}(s; q^2)$ can be written as

$$\mathcal{Z}_{l\neq 0,m}(s; q^2) = \sum_{|\mathbf{n}|<\Lambda} \frac{1}{(\mathbf{n}^2 - q^2)^s} \mathcal{Y}_{lm}(\mathbf{n})$$

$$+ \frac{(2\pi)^3}{\Gamma(s)} \left\{ \int_0^1 t^{s-1} t^{q^2} \mathcal{K}^{\Lambda}_{lm}(t, \vec{0}) dt + \int_1^{\infty} t^{s-1} t^{q^2} \mathcal{K}^{\Lambda}_{lm}(t, \vec{0}) dt \right\} \tag{109}$$

A general expression including the $\mathcal{Z}_{00}$ case is

$$
\begin{aligned}
&\mathcal{Z}_{lm}(s;q^2) \\
&= \sum_{|\mathbf{n}|<\Lambda} \frac{1}{(\mathbf{n}^2-q^2)^s}\mathcal{Y}_{lm}(\mathbf{n}) && \text{Finite sum term} \\
&+ \frac{(2\pi)^3}{\Gamma(s)}\left\{ \frac{\delta_{l0}\delta m_0}{(4\pi)^2(s-\frac{3}{2})} \right. && \text{Asymptotic term} \\
&\quad \left. + \int_0^1 t^{s-1}\left[t^{q^2}\mathcal{K}^{\Lambda}_{lm}(t,\vec{0}) - \frac{\delta_{l0}\delta m_0}{(4\pi)^2 t^{\frac{3}{2}}}\right]dt + \int_1^\infty t^{s-1}t^{q^2}\mathcal{K}^{\Lambda}_{lm}(t,\vec{0})dt \right\} && \text{Integral term}
\end{aligned}
\tag{110}
$$

where the Kronecker delta $\delta_{l0}\delta m_0$ is used to include the asymptotic behaviour for the $\mathcal{Z}_{00}$ case. The Zeta function is split into three parts, finite sum term, asymptotic term and integral term. The substitution of truncated heat kernels is in the same manner as in Eq. 82.

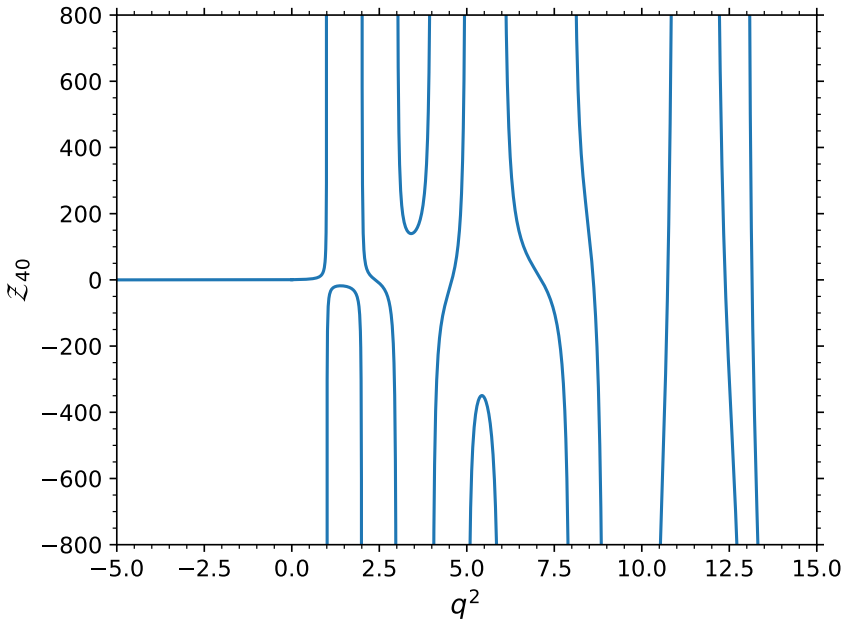

Figure 3: Plot of the Zeta function $\mathcal{Z}_{40}(1;q^2)$

Fig. 3 shows the plot of the Zeta function $\mathcal{Z}_{40}(1;q^2)$ for $q^2 \in [-5,15]$. We observe a similar asymptotic behavior as in the $\mathcal{Z}_{00}$ case, where the Zeta function diverges at $q^2 = \mathbf{n}^2$. Due to the presence of the term $\mathcal{Y}_{40}(\mathbf{n})$ in the sum, the behavior of the Zeta function $\mathcal{Z}_{40}(1;q^2)$ varies across different continuous regions of q^2, exhibiting parabolic, cubic, or other complex characteristics.

2.2.2 Leskovec's method

Leskovec's derivation of the Zeta function $\mathcal{Z}_{lm}(s;q^2)$ slightly differs from the Luscher's method in its handling of the order of applying the Gamma function and splitting of the integral [10]

Using the Gamma function $\Gamma(s)$ in Eq. 41 first and splitting the integral into two parts at $t=1$, the Zeta function $\mathcal{Z}_{lm}(s;q^2)$ can be written as

$$\mathcal{Z}_{lm}(s;q^2) = \frac{1}{\Gamma(s)} \sum_{\mathbf{n}\in\mathbb{Z}^3} \mathcal{Y}_{lm}(\mathbf{n}) \int_0^\infty t^{s-1} e^{-t(\mathbf{n}^2-q^2)} dt \tag{111}$$

$$= \frac{1}{\Gamma(s)} \sum_{\mathbf{n}\in\mathbb{Z}^3} \mathcal{Y}_{lm}(\mathbf{n}) \left\{ \int_0^1 t^{s-1} e^{-t(\mathbf{n}^2-q^2)} dt + \int_1^\infty t^{s-1} e^{-t(\mathbf{n}^2-q^2)} dt \right\} \tag{112}$$

The second term in Eq. 112 can be evaluated at $s=1$ and yields a finite sum

$$\frac{1}{\Gamma(s)} \sum_{\mathbf{n}\in\mathbb{Z}^3} \mathcal{Y}_{lm}(\mathbf{n}) \int_1^\infty t^{s-1} e^{-t(\mathbf{n}^2-q^2)} dt = \sum_{\mathbf{n}\in\mathbb{Z}^3} \mathcal{Y}_{lm}(\mathbf{n}) \int_1^\infty e^{-t(\mathbf{n}^2-q^2)} dt \tag{113}$$

$$= \sum_{\mathbf{n}\in\mathbb{Z}^3} \mathcal{Y}_{lm}(\mathbf{n}) \frac{e^{-(\mathbf{n}^2-q^2)}}{\mathbf{n}^2-q^2} \tag{114}$$

This expression ensures faster convergence with exponential decay on the difference $\mathbf{n}^2 - q^2$.

The first term in Eq. 112 can be rearranged to

$$\frac{1}{\Gamma(s)} \sum_{\mathbf{n}\in\mathbb{Z}^3} \mathcal{Y}_{lm}(\mathbf{n}) \int_0^1 t^{s-1} e^{-t(\mathbf{n}^2-q^2)} dt = \frac{1}{\Gamma(s)} \int_0^1 t^{s-1} e^{tq^2} \sum_{\mathbf{n}\in\mathbb{Z}^3} \mathcal{Y}_{lm}(\mathbf{n}) e^{-t\mathbf{n}^2} dt \tag{115}$$

such that we can apply the Poisson summation formula to the summation following the same procedure from Eq. 85 to Eq. 106. This yields

$$\frac{1}{\Gamma(s)} \sum_{\mathbf{n}\in\mathbb{Z}^3} \mathcal{Y}_{lm}(\mathbf{n}) \int_0^1 t^{s-1} e^{-t(\mathbf{n}^2-q^2)} dt$$

$$= \frac{1}{\Gamma(s)} \int_0^1 t^{s-1} e^{tq^2} \sum_{\mathbf{n}\in\mathbb{Z}^3} (-i)^l \mathcal{Y}_{lm}\left(\frac{\pi\mathbf{n}}{t}\right) \left(\frac{\pi}{t}\right)^{\frac{3}{2}} \exp\left(-\frac{\pi^2\mathbf{n}^2}{t}\right) dt \tag{116}$$

This integral is finite for all $\mathbf{n}$ except for $\mathbf{n}^2 = 0$ for $s=1$ case. The divergence occurs only when $l=m=0$ since the term $\mathcal{Y}_{lm}$ evaluated at origin is non-zero.

$$\mathcal{Y}_{lm}(\mathbf{n}=0) = |r|^l Y_{lm}(\theta,\phi) = \begin{cases} \frac{1}{\sqrt{4\pi}} & \text{for} \quad l=0, m=0 \\ 0 & \text{otherwise} \end{cases} \tag{117}$$

The $\mathbf{n} = 0$ in Eq. 116 is

$$\frac{1}{\Gamma(s)} \frac{\pi^{\frac{3}{2}}}{\sqrt{4\pi}} \int_0^1 t^{s-\frac{5}{2}} e^{tq^2} dt \tag{118}$$

and its divergence for $s = 1$ can be evaluated using analytic continuation by separating it into two parts

$$\int_0^1 t^{s-\frac{5}{2}} e^{tq^2} = \int_0^1 t^{s-\frac{5}{2}} (e^{tq^2} - 1) dt + \int_0^1 t^{s-\frac{5}{2}} dt \tag{119}$$

The second integral is -2 as described in Eq. 79, while the first integral is now convergent. The $\mathbf{n} = 0$ term at $s = 1$ is then

$$\frac{1}{\Gamma(s)} \frac{\pi^{\frac{3}{2}}}{\sqrt{4\pi}} \int_0^1 t^{s-\frac{5}{2}} e^{tq^2} dt = \frac{\pi}{2} \left[\int_0^1 t^{-\frac{3}{2}} (e^{tq^2} - 1) dt - 2 \right] \tag{120}$$

$$= \frac{\pi}{2} \int_0^1 t^{-\frac{3}{2}} (e^{tq^2} - 1) dt - \pi \tag{121}$$

Therefore, collecting from Eq. 114, Eq. 116 and Eq. 118, the Zeta function $\mathcal{Z}_{lm}(s = 1; q^2)$ is

$$\begin{aligned}
&\mathcal{Z}_{lm}(s = 1; q^2) \\
&= \sum_{\mathbf{n} \in \mathbb{Z}^3} \mathcal{Y}_{lm}(\mathbf{n}) \frac{e^{-(\mathbf{n}^2 - q^2)}}{\mathbf{n}^2 - q^2} && \text{Finite sum term} \\
&+ \int_0^1 e^{tq^2} \sum_{\mathbf{n} \in \mathbb{Z}^3, \mathbf{n} \neq \vec{0}} (-i)^l \mathcal{Y}_{lm} \left(\frac{\pi \mathbf{n}}{t} \right) \left(\frac{\pi}{t} \right)^{\frac{3}{2}} \exp \left(-\frac{\pi^2 \mathbf{n}^2}{t} \right) dt && \text{Integral term} \\
&+ \delta_{l0} \delta_{m0} \left[\frac{\pi}{2} \int_0^1 t^{-\frac{3}{2}} (e^{tq^2} - 1) dt - \pi \right] && \text{Asymptotic term}
\end{aligned} \tag{122}$$

which consists of three terms: finite sum term, integral term, and asymptotic term. This equation contains exponential accelerated terms for faster convergence and is now suitable for numerical evaluation.

2.2.3 Savage's method

Savage's method mirrors Leskovec's approach, differing only in the treatment of the analytic continuation of $\mathcal{Z}_0 0$ [21, 22]. We commence with Eq. 118. Instead of using the analytic continuation by subtracting off the divergence directly, we evaluate this integral first for $\Re s > \frac{3}{2}$

$$\frac{1}{\Gamma(s)} \frac{\pi^{\frac{3}{2}}}{\sqrt{4\pi}} \int_0^1 t^{s-\frac{5}{2}} e^{tq^2} dt \tag{123}$$

Applying the integral by parts relation $\int uv\prime dx = uv - \int u\prime v dx$, we set $u = e^{tq^2}$ and $v\prime = t^{s-\frac{5}{2}}$. This yields

$$\frac{1}{\Gamma(s)}\frac{\pi^{\frac{3}{2}}}{\sqrt{4\pi}}\int_0^1 t^{s-\frac{5}{2}}e^{tq^2}dt = \frac{1}{\Gamma(s)}\frac{\pi}{2}\left\{\left[e^{tq^2}\ \frac{1}{s-\frac{3}{2}}t^{s-\frac{3}{2}}\right]_0^1 - \int_0^1 e^{tq^2}q^2\frac{1}{s-\frac{3}{2}}t^{s-\frac{3}{2}}dt\right\} \tag{124}$$

$$= \frac{1}{\Gamma(s)}\frac{\pi}{2}\frac{e^{q^2}}{s-\frac{3}{2}} - \frac{1}{\Gamma(s)}\frac{\pi}{2}\int_0^1 e^{tq^2}q^2\frac{1}{s-\frac{3}{2}}t^{s-\frac{3}{2}}dt \tag{125}$$

The divergence for $s = 1$ remains in the integral. To address this issue, we can apply the integral by parts one more. By setting $u = e^{tq^2}$ and $v\prime = t^{s-\frac{3}{2}}$, we obtain

$$\frac{1}{\Gamma(s)}\frac{\pi}{2}\int_0^1 e^{tq^2}q^2\frac{1}{s-\frac{3}{2}}t^{s-\frac{3}{2}}dt \tag{126}$$

$$= \frac{1}{\Gamma(s)}\frac{\pi}{2}q^2\frac{1}{s-\frac{3}{2}}\left\{\left[e^{tq^2}\frac{1}{s-\frac{1}{2}}t^{s-\frac{1}{2}}\right]_0^1 - \int_0^1 e^{tq^2}\frac{1}{s-\frac{1}{2}}t^{s-\frac{1}{2}}dt\right\} \tag{127}$$

$$= \frac{1}{\Gamma(s)}\frac{\pi}{2}q^2\left[\frac{1}{s-\frac{3}{2}}\frac{e^{q^2}}{s-\frac{1}{2}} - \frac{1}{s-\frac{3}{2}}\int_0^1 e^{tq^2}q^2\frac{1}{s-\frac{1}{2}}t^{s-\frac{1}{2}}dt\right] \tag{128}$$

Collecting Eq. 125 and Eq. 128, the $\mathbf{n} = 0$ term as presented in Eq. 118 is

$$\frac{1}{\Gamma(s)}\frac{\pi^{\frac{3}{2}}}{\sqrt{4\pi}}\int_0^1 t^{s-\frac{5}{2}}e^{tq^2}dt = \frac{1}{\Gamma(s)}\frac{\pi}{2}\frac{e^{q^2}}{s-\frac{3}{2}} - \frac{1}{\Gamma(s)}\frac{\pi}{2}q^2\left[\frac{1}{s-\frac{3}{2}}\frac{e^{q^2}}{s-\frac{1}{2}} - \frac{1}{s-\frac{3}{2}}\int_0^1 e^{tq^2}q^2\frac{1}{s-\frac{1}{2}}t^{s-\frac{1}{2}}dt\right] \tag{129}$$

Analytic continuation to $s = 1$ gives

$$\frac{\pi^{\frac{3}{2}}}{\sqrt{4\pi}}\int_0^1 t^{-\frac{3}{2}}e^{tq^2}dt = \frac{\pi}{2}\frac{e^{q^2}}{-\frac{1}{2}} - \frac{\pi}{2}q^2\left[\frac{1}{-\frac{1}{2}}\frac{e^{q^2}}{\frac{1}{2}} - \frac{1}{-\frac{1}{2}}\int_0^1 e^{tq^2}\frac{1}{\frac{1}{2}}t^{\frac{1}{2}}dt\right] \tag{130}$$

$$= -\pi e^{q^2} + 2\pi e^{q^2}q^2 - \frac{\pi}{2}\int_0^1 e^{tq^2}4q^4t^{\frac{1}{2}}dt \tag{131}$$

Therefore, by inserting $\mathcal{Y}_{00} = \frac{1}{\sqrt{4\pi}}$, the Zeta function $\mathcal{Z}_{00}(s=1;q^2)$ is

$$\begin{aligned}
&\mathcal{Z}_{00}(s=1;q^2) \\
&= \sum_{\mathbf{n}\in\mathbb{Z}^3} \frac{1}{\sqrt{4\pi}} \frac{e^{-(\mathbf{n}^2-q^2)}}{\mathbf{n}^2-q^2} && \text{Finite sum term} \\
&+ \frac{\pi}{2}\int_0^1 e^{tq^2} \sum_{\mathbf{n}\in\mathbb{Z}^3,\mathbf{n}\neq\vec{0}} \left(\frac{1}{t}\right)^{\frac{3}{2}} \exp\left(-\frac{\pi^2\mathbf{n}^2}{t}\right) dt && \text{Integral term} \\
&- \pi e^{q^2} + 2\pi e^{q^2} q^2 - \frac{\pi}{2}\int_0^1 e^{tq^2} 4q^4 t^{\frac{1}{2}} dt && \text{Asymptotic term} \qquad (132)
\end{aligned}$$

The Zeta function $\mathcal{Z}_{lm}(s=1;q^2)$ for $l \neq 0$ is the same as Leskovec's method.

2.2.4 Summary of methods

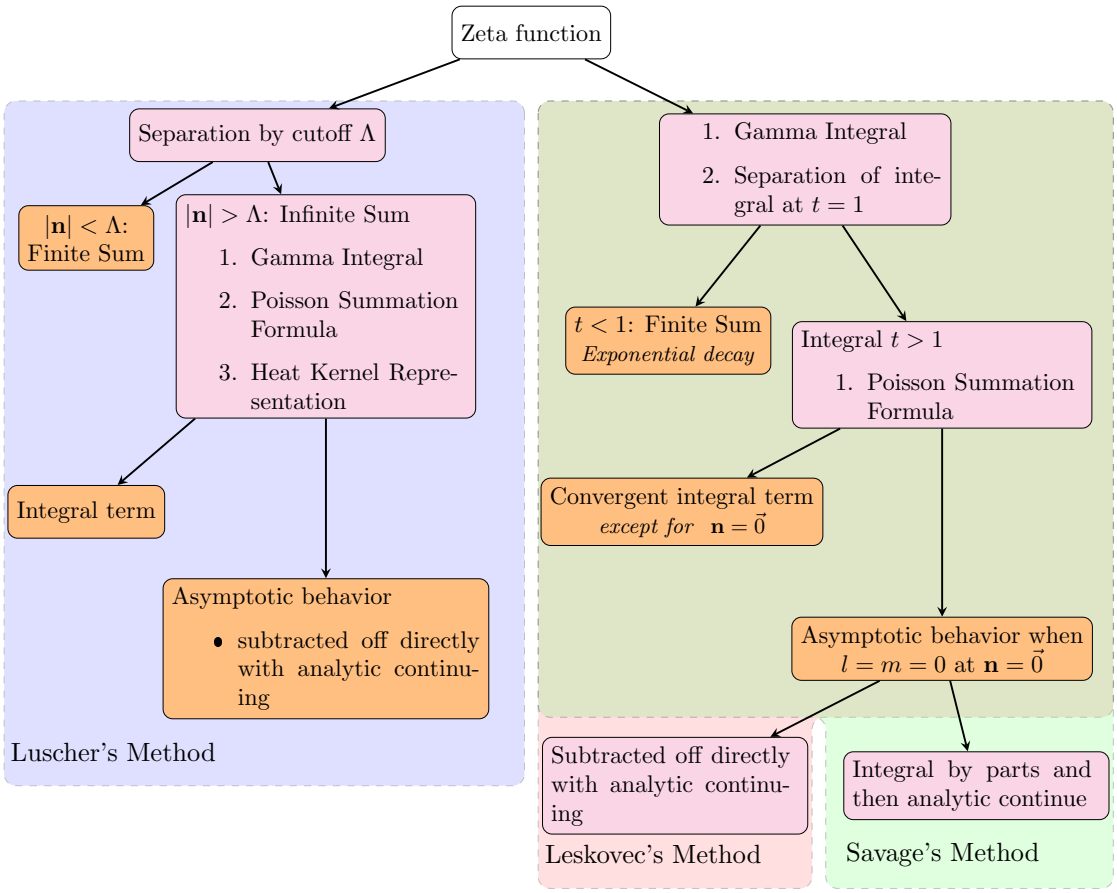

Figure 4: Summary of methods for evaluating the Zeta function $\mathcal{Z}_{lm}(s;q^2)$. The pink nodes represent the operations on the Zeta function, while the orange nodes represent a term in the alternative representation of the Zeta function. The dashed boxes represent the operations/terms involved in each method.

As depicted in Fig. 4, the alternative representations of the Zeta function all employ the Gamma integral and Poisson summation formula. The key difference lies in the separation of the Zeta function into a finite sum and an integral term. Luscher's method directly splits the original summation in the Zeta function, while Leskovec's and Savage's methods separate the Gamma integral at $t = 1$. The finite sum for Leskovec's and Savage's methods has an exponential decay coefficient, ensuring faster convergence. The asymptotic behavior appears in the integral term for all methods. Luscher's and Leskovec's methods subtract off the divergence directly and analytically continue the divergence to $s = 1$. In contrast, Savage's method uses integration by parts to evaluate the divergent integral first in the real half plane $\Re s > \frac{3}{2}$ before performing the analytic continuation to $s = 1$. Among these methods, the analytic continuation is crucial to

define further values of a function, for example, $s = 1$ in the Zeta function where the infinite series representation which was well defined for $\Re s > \frac{3}{2}$ becomes divergent.

2.3 Simplification and performance considerations

2.3.1 Simplification for $\mathcal{Z}_{00}$

In the case of $\mathcal{Z}_{00}$, the Zeta function is independent of the azimuthal angle ϕ and the polar angle θ, where the spherical harmonics $Y_{00}(\theta, \phi)$ yields a constant. The Zeta function only depends on the magnitude of the relative position vector $r = |\mathbf{r}|$. Specifically when taking the sum over the lattice, only the first octant in the 3D space needs to be evaluated, whereas the contributions in other octants can be obtained by symmetry considerations. The symmetry coefficient is 2^m where m is the number of non-zero values in the vector $\mathbf{n} = (n_1, n_2, n_3)^T$. The symmetry simplification can be applied to both the finite sum term and the integral term, thereby reducing the number of evaluations by 1/8.

However, such a symmetry simplification over the mesh is not applied to $l \neq 0$ cases, despite the fact that the term $\mathcal{Y}_{lm}(\theta, \phi)$ exhibits certain symmetries that vary with different l. This is the balance between the coding complexity and the performance gain.

2.3.2 Simplification for $\mathcal{Z}_{lm}$ with $l \neq 0$

In higher partial waves, the Zeta function can be simplified by utilizing symmetric properties of the term $\mathcal{Y}_{lm}$ [23]. In particular, the following transformations can be applied to simplify the Zeta function evaluation

1. Parity transformation $\mathbf{x} \to -\mathbf{x}$

$$\mathcal{Z}_{lm}(1; q^2) = 0 \quad \text{if} \quad l \quad \text{is odd} \tag{133}$$

2. Reflection symmetry $\mathbf{x} \to (x_1, -x_2, x_3)^T$

$$\mathcal{Z}_{lm}(1; q^2) = \mathcal{Z}_{l,-m}(1; q^2) \tag{134}$$

3. Rotation about x_3-axis with angle $\pi/2$

$$\mathcal{Z}_{lm} = 0 \quad \text{if} \quad m \neq 4n, n \in \mathbb{Z} \tag{135}$$

These properties reduce computation cost for the same q^2 values but at different l, m values. They also simplify the number of Zeta functions involved in the matrix M, providing a simplified form.

In the stationary frame, additional symmetries can be exploited due to the cubic symmetry [23]. In particular,

$$\mathcal{Z}_{20}(1;q^2) = 0 \tag{136}$$

$$\mathcal{Z}_{44}(1;q^2) = \frac{\sqrt{70}}{14}\mathcal{Z}_{40}(1;q^2) \tag{137}$$

For example, the matrix M in Eq. 20 for $l_{max} = 1$ is a 4×4 matrix with basis $lm = 00; 10; 11; 1-1$ as shown below

$$M_{lm,l'm'} = \begin{array}{c} \\ 00 \\ 10 \\ 11 \\ 1-1 \end{array} \begin{array}{c} \begin{array}{cccc} 00 & 10 & 11 & 1-1 \end{array} \\ \begin{pmatrix} w_{00} & i\sqrt{3}w_{10} & i\sqrt{3}w_{11} & i\sqrt{3}w_{1-1} \\ -i\sqrt{3}w_{10} & w_{00}+2w_{20} & \sqrt{3}w_{21} & \sqrt{3}w_{2-1} \\ i\sqrt{3}w_{1-1} & -\sqrt{3}w_{2-1} & w_{00}-w_{20} & -\sqrt{6}w_{2-2} \\ i\sqrt{3}w_{11} & -\sqrt{3}w_{21} & -\sqrt{6}w_{22} & w_{00}-w_{20} \end{pmatrix} \end{array} \tag{138}$$

with the coefficient $w_{lm} = \frac{1}{\pi^{\frac{3}{2}}\sqrt{2l+1}q^{l+1}}\mathcal{Z}_{lm}(1;q^2)$. Applying the symmetry properties in the stationary frame, the matrix M is a diagonal matrix with 4-fold degeneracy of eigenvalue w_{00}, in agreement with Eq. 38.

Here, we present a series of Zeta functions with higher partial waves $l \neq 0$ that are non-zero in the stationary frame. Fig. 5 shows the Zeta function $\mathcal{Z}_{44}(1;q^2)$. Fig 6 and Fig 7 show the Zeta function $\mathcal{Z}_{lm}(1;q^2)$ for $l = 6$ with $m = 0, 4$, respectively. The asymptotic behavior at $q^2 = 0$ is a pole because the term $\mathcal{Y}_{lm}(\vec{0})$ is zero, making the zeta function sum term $\mathcal{Y}_{lm}(\vec{0})\frac{e^{-q^2}}{q^2}$ undefined at this point. More plots for the Zeta function $\mathcal{Z}_{lm}(1;q^2)$ can be found in Appendix A.

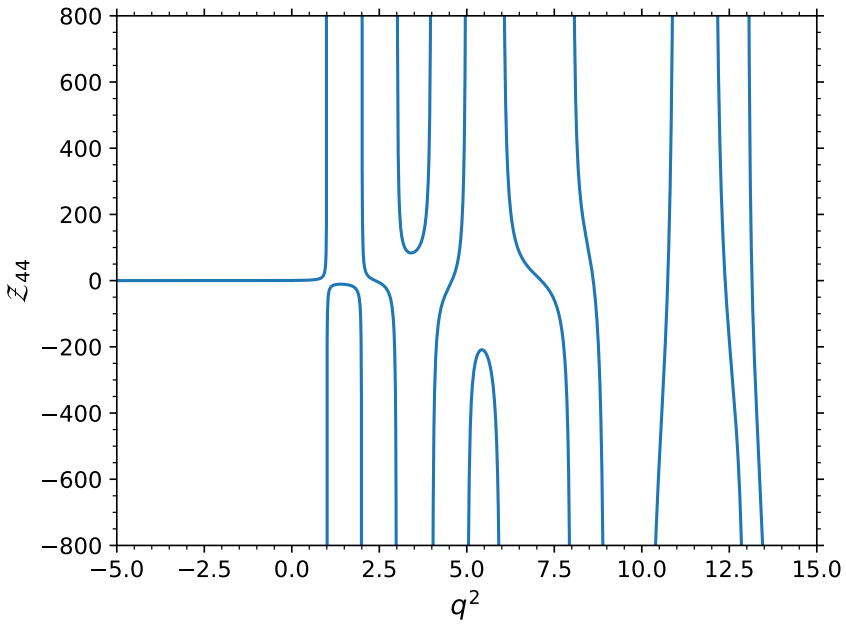

Figure 5: Plot of the Zeta function $\mathcal{Z}_{44}(1; q^2)$

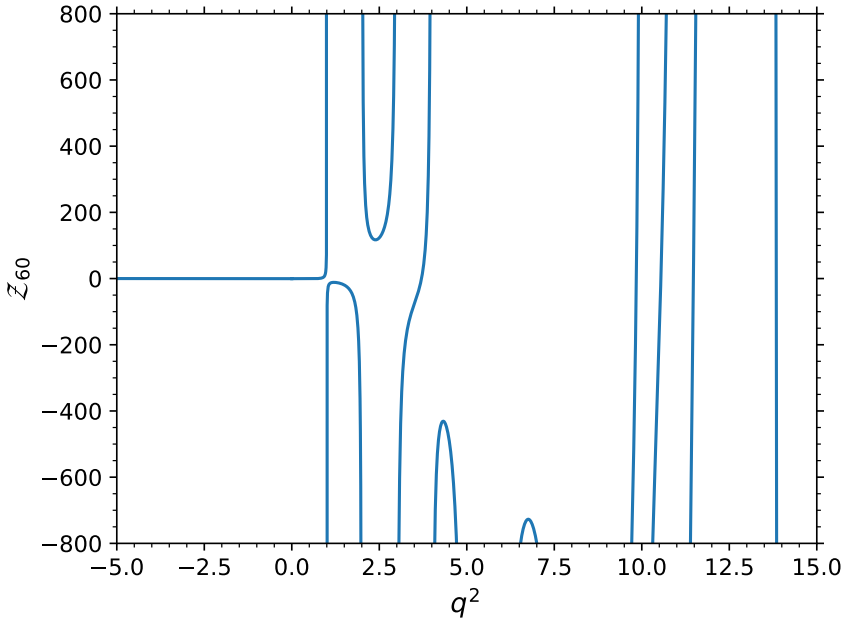

Figure 6: Plot of the Zeta function $\mathcal{Z}_{60}(1; q^2)$

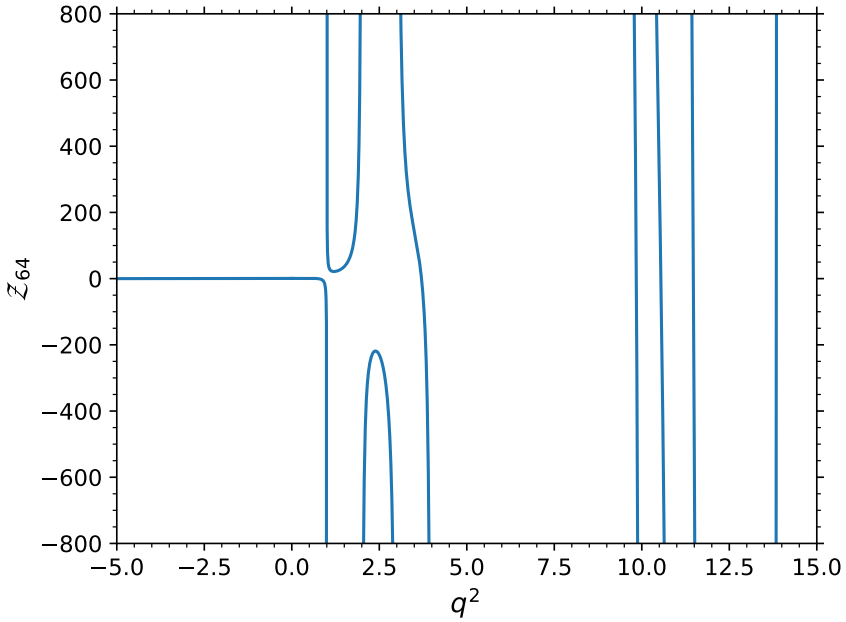

Figure 7: Plot of the Zeta function $\mathcal{Z}_{64}(1; q^2)$

2.3.3 Change of variables

In Luscher's Zeta function, as given in Eq. 81, the integrals may converge slowly, which can cause `scipy.integrate` to complain and require more function evaluations. To speed up the convergence, we can apply the change of variables (CoV).

For the integral from 0 to 1, since the integral diverges at $t = 0$, a useful CoV is the square root function

$$\int_a^b f(t)dt = \int_{x=0}^{x=\sqrt{b-a}} 2xf(a + x^2)dx \quad \text{for} \quad b > a \tag{139}$$

This transformation addresses the singularity at a [24].

The effect of this CoV on the number of evaluations is shown in Fig. 8. This transformation reduces the number of evaluations by $\approx 1/10$. Although the CoV does not change the nature of the singularity, in which a large number of evaluations around the singularity $t = 0$ is still required, it speeds up the integral convergence by redistributing the evaluation points more evenly and accelerates the integral convergence.

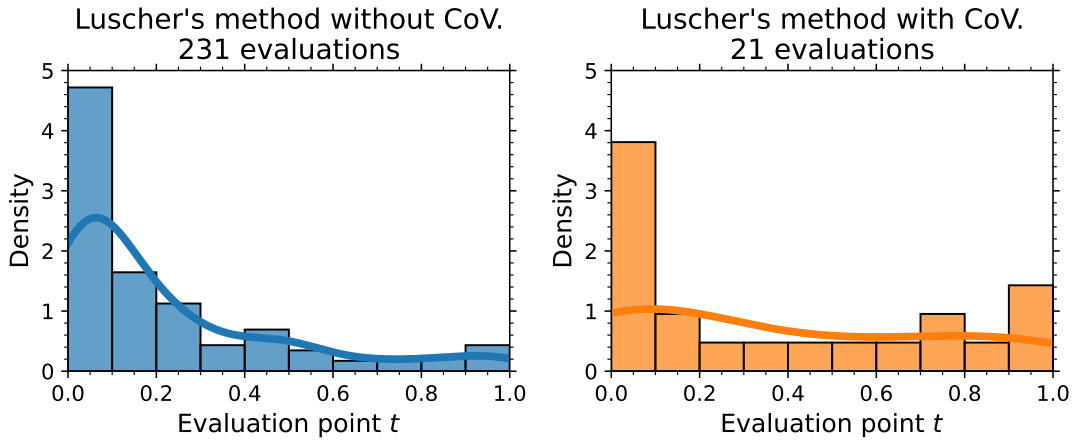

Figure 8: Comparison of the Zeta function $\mathcal{Z}_{00}(1;q^2)$ evaluation points for the integral $t \in (0,1)$ and $q^2 = 0.5$ with and without CoV.

However, for cases where $l \neq 0$, the CoV does not significantly simplify the number of evaluations, but it does not complicate them either, as shown in Fig. 9. The CoV can still be beneficial, as it slightly reduces the actual integration error under the same number of evaluations. The significance of applying CoV depends on the cutoff Λ, where the summation of the points with $|\mathbf{n}| < \Lambda$ affects the convergence of the integral term.

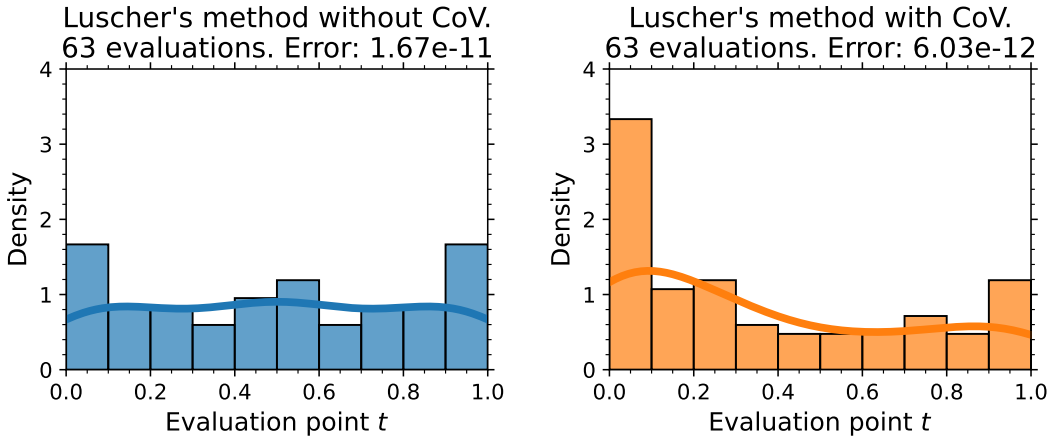

Figure 9: Comparison of the Zeta function $\mathcal{Z}_{60}(1;q^2)$ evaluation points for the integral $t \in (0,1)$ and $q^2 = 0.5$ with and without CoV.

For the integral over the interval $t \in (1,+\infty)$, we can apply the CoV using the exponen-

tial relation $t = e^{-x}$ due to the rapid fall-off of the integrand [24].

$$\int_{t=a}^{t=+\infty} f(t)dt = \int_{x=0}^{x=e^{-a}} f(-\log x)\frac{dx}{x} \tag{140}$$

The CoV technique can also be used in other derivations, like Savage's method in Sec. 2.2.3 and Leskovec's method in Sec. 2.2.2, to improve the convergence of the integral term.

2.3.4 Convergence test

Luscher's method The cutoff λ should be chosen as close to the the lower bound $|q^2|$. This minimizes the number of terms for the summation in both the finite sum term and the integral term.

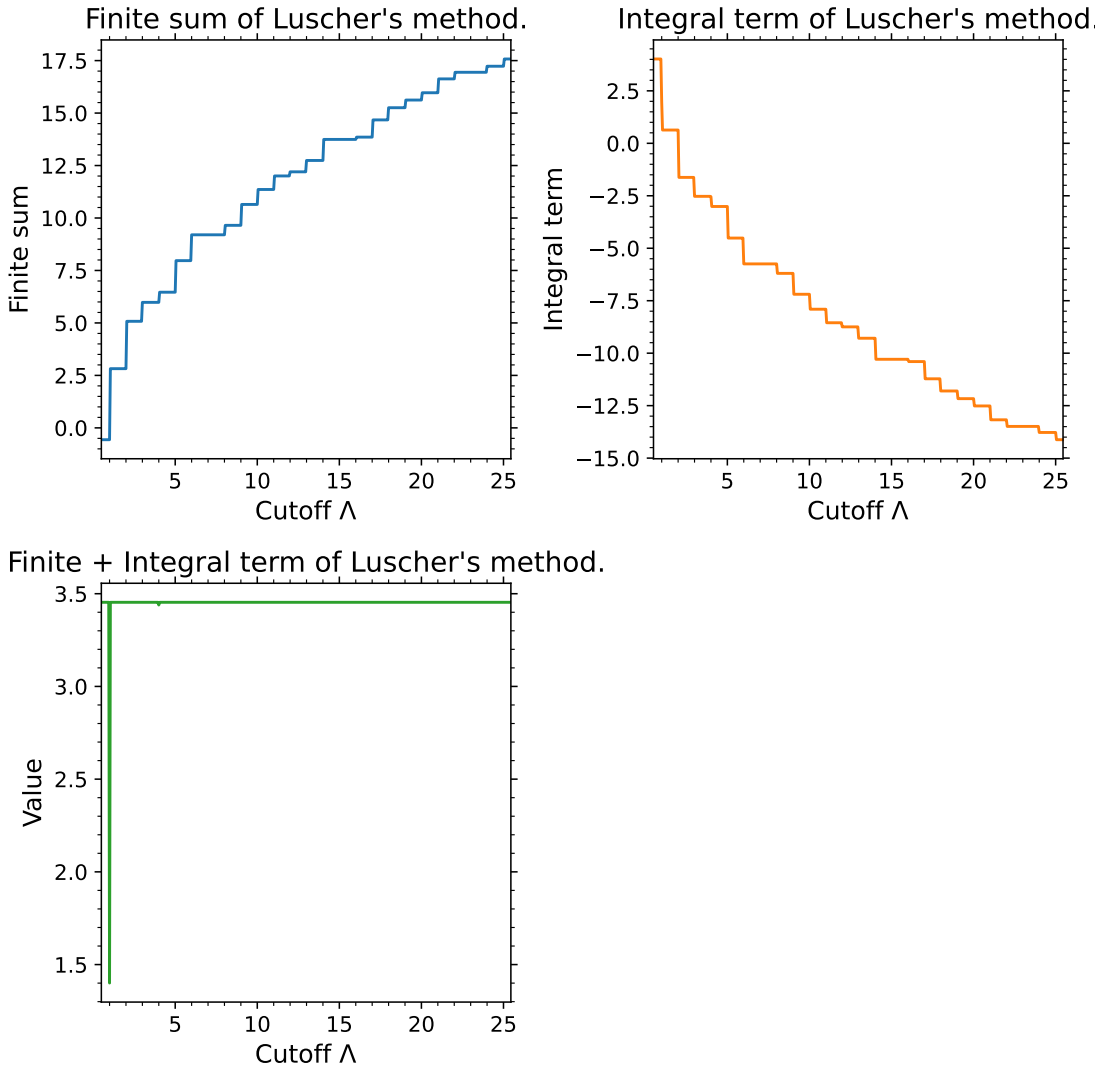

Figure 10: Convergence test for the Zeta function $\mathcal{Z}_{00}(1;q^2)$ using Luscher's method. The convergence is tested for different cutoff Λ values.

In the $\mathcal{Z}_{00}$ case, the finite term and the integral term value with respect to the cutoff Λ is shown in Fig. 10. As the cutoff Λ increases, we expect both the finite sum term and the integral term to approach a constant value, However, the sum of these two terms converges as the cutoff Λ increases. This is due to the contribution of values that exist in the finite sum term or the integral term depending on the cutoff Λ.

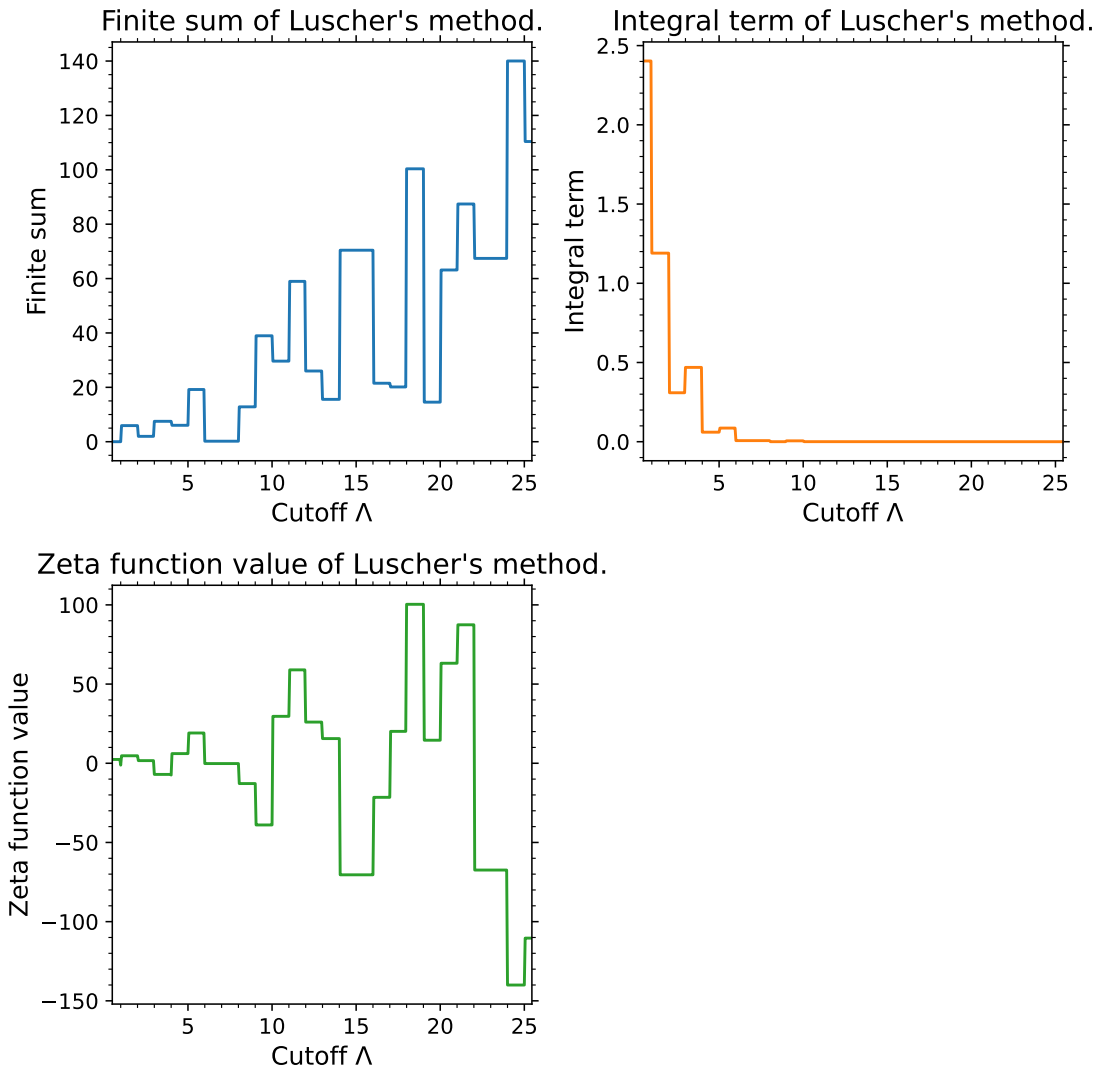

Figure 11: Convergence test for the Zeta function $\mathcal{Z}_{40}(1;q^2)$ using Luscher's method. The convergence is tested for different cutoff Λ values.

A different behavior is observed in the $\mathcal{Z}_{40}$ case, as shown in Fig. 11. The integral term is convergent, but the finite sum term is increasing and oscillating. This behavior is related to the points mesh involved. As the cutoff Λ increases, the power of the magnitude of the point $|\mathbf{n}|^l$ in the spherical harmonics Eq 24 increases exponentially. Additionally, the sign of the summation term depends on both the spherical harmonics and the denominator $\mathbf{n}^2 - q^2$, which introduces the oscillatory behavior. The cutoff Λ can not guarantee a convergence. In practice, the cutoff Λ should be chosen as close to the lower bound $|q^2|$ to ensure numerical stability.

In Fig. 10 and 11, the maximum cutoff is $\Lambda = 25$, there are already $25^3 = 15625$ points involved for summing $\mathbf{n}$. This is computationally expensive, and the convergence is not guaranteed at this level for higher partial waves.

Leskovec's method Leskovec's method and Savage's method have the same finite sum term and integral term. The different asymptotic term does not involve any $\mathbf{n}$ dependence. For convergence evaluation, we adopt a cutoff parameter Λ, mirroring Luscher's approach.

Fig. 12 illustrates the convergence test for the Zeta function $\mathcal{Z}_{00}(1; q^2)$ using Leskovec's method. As the cutoff Λ increases, both the finite sum term and the integral term reach a plateau, benefitting from the rapid convergence facilitated by the exponential decays $e^{-(\mathbf{n}^2 - q^2)}$ in the finite sum term and $\exp\left(-\frac{\pi^2 \mathbf{n}^2}{t}\right)$ in the integral term.

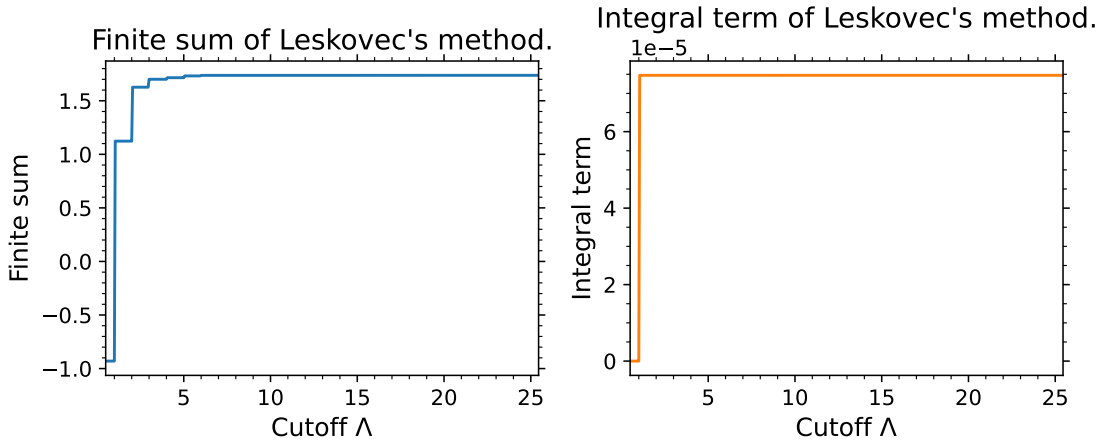

Figure 12: Convergence test for the Zeta function $\mathcal{Z}_{00}(1; q^2)$ using Leskovec's method. The convergence is tested for different cutoff Λ values.

A faster convergence for the $\mathcal{Z}_{40}$ case is observed in Fig. 13. For Leskovec's method, in general, the integral term converges faster than the finite sum term, because the exponential decay term in the integral has a faster decay as it is enlarged by factor $\frac{1}{t}$ in the exponential term for $t \in (0, 1)$. The finite sum term requires more points to meet the convergence criteria.

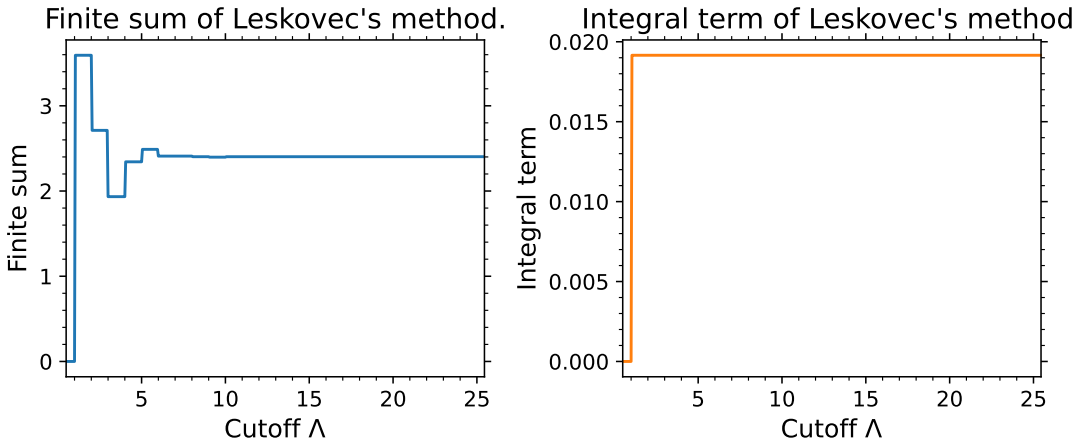

Figure 13: Convergence test for the Zeta function $\mathcal{Z}_{40}(1;q^2)$ using Leskovec's method. The convergence is tested for different cutoff Λ values.

When evaluating the Zeta function with a specific tolerance τ requirement, we can find the minimum required $\mathbf{n}^2$. In the finite sum part of the $\mathcal{Z}_{00}$ case, the finite summand is

$$\mathcal{Y}_{00}(\mathbf{n})\frac{e^{-(\mathbf{x}^2)}}{\mathbf{x}^2} = \tau \tag{141}$$

where $\mathbf{x}^2 = \mathbf{n}^2 - q^2$. Taking the logarithm on both sides and rearranging the terms,

$$\frac{1}{\sqrt{4\pi}}\frac{e^{-\mathbf{x}^2}}{\mathbf{n}^2 - q^2} = \tau \tag{142}$$

$$-\log\sqrt{4\pi} - \mathbf{x}^2 - \log(\mathbf{x}^2) = \log\tau \tag{143}$$

This equation is now suitable for a root-finding algorithm to find the minimum required $\mathbf{x}^2$ for a specific tolerance τ. The estimation of the minimum required $\mathbf{n}^2$ can reduce the summation to two times, one for evaluating the summand and one for ensuring the tolerance is met.

The Zeta $\mathcal{Z}_{00}$ function results are tested against the phase information $\delta/\pi q^2$ in Table A.1 of Luscher's paper [25]. For higher partial wave phase shifts, the results are compared against the digitized data from the figures in Savage's paper [21].

In summary, Luscher's method is convergent for almost any cutoff Λ in $\mathcal{Z}_{00}$ case, but diverges for individual terms and fails for higher partial wave. On the other hand, Leskovec's method is convergent in both finite sum term and integral term for all cases, though requiring a slightly larger cutoff. This makes Leskovec's method particularly well-suited for precise numerical evaluations.

2.3.5 Performance for different implementations

Among the alternative expressions proposed by Luscher, Leskovec, and Savage for the Zeta function, the finite sum component does not introduce significant numerical complexity. which is about $\mathcal{O}(n_{mesh})$ for n_{mesh} points in the mesh. The complexity arises from the integral term, where the integrand is coupled with the summation over the mesh, leading to a complexity about $\mathcal{O}((n_{mesh})^{n_{subinterval}})$ for $n_{subinterval}$ sub-interval evaluations. The computational cost for evaluating the Zeta function is dominated by the number of evaluations required for this integral term.

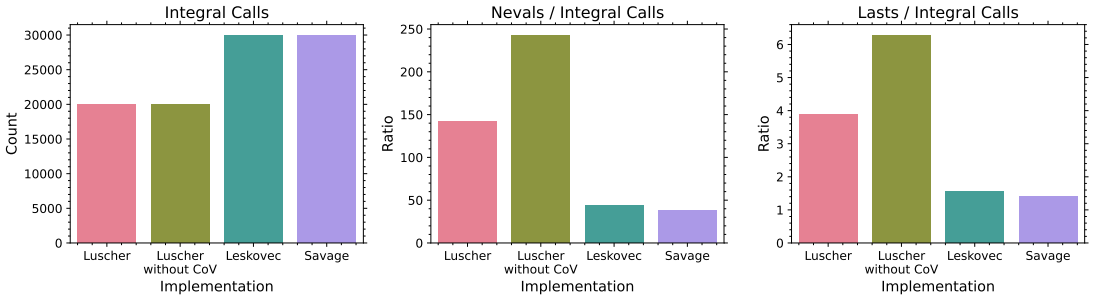

Figure 14: Comparison of integral calls for the Zeta function $\mathcal{Z}_{00}(1; q^2)$ for 10k q^2 using Luscher's, Leskovec's, and Savage's methods.

Fig. 14 compares the integration calls, the average number of integrand evaluations and the average subintervals produced in the subdivision process using the quadrature rule of integration for different implementations. As discussed in Sec. 2.3.3, the CoV technique greatly reduces the number of evaluations for Luscher's method by modifying the asymptotic behavior of the integrand and hence changing the distribution of the subintervals.

In contrast to Luscher's method, Leskovec and Savage's methods exhibit a higher number of integral calls. This disparity is expected, as an additional integral evaluation ensures convergence in Leskovec's and Savage's methods, which is a feature absent in Luscher's method.

The average number of evaluations of t in Leskovec's and Savage's methods is significantly lower than in Luscher's method, owing to the faster convergence of the integral term. Savage's method slightly outperforms Leskovec's due to the difference in analytic continuing the asymptotic integral term.

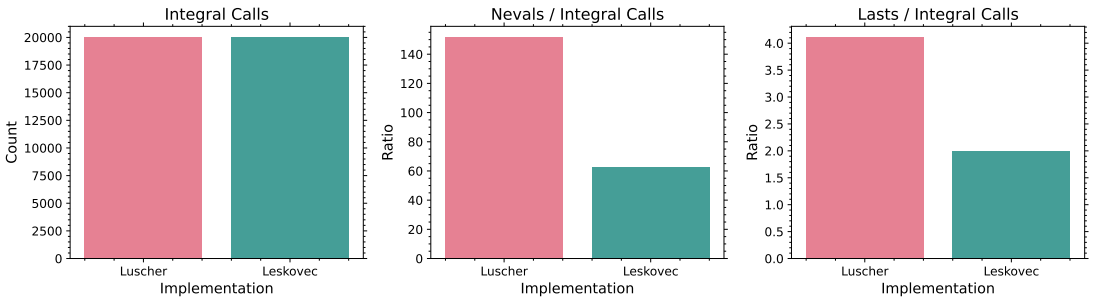

Figure 15: Comparison of integral calls for the Zeta function $\mathcal{Z}_{40}(1; q^2)$ for 10k q^2 using Luscher's and Leskovec's methods.

Figure 15 presents a similar result for the Zeta function $\mathcal{Z}_{40}(1; q^2)$ using Luscher's and Leskovec's methods.

To efficiently evaluate the Zeta function over a series of q^2 values, parallel computation using Python's `multiprocessing` module is employed. The dominant computation cost occurs in evaluating the integral term with a summation of mesh points $\mathbf{n}$.

In short, Leskovec's method or Savage's method is preferred for numerical evaluation due to the faster convergence and less computation cost. Leskovec's method will be utilized for evaluating the Zeta function in subsequent sections.

3 Application: Pion-pion scattering phase shift at stationary frame

One practical for the Zeta function is to study the resonances that decay via strong interactions. Among these resonance behaviors, the ϕ meson is an ideal candidate for lattice simulation because of its precise numerical determination of mass with small statistical errors and its decay channel primarily to a pair of pions, which can be treated on the lattice very precisely [5].

3.1 Evaluation of result

Table 1 presents the energy of the pion-pion scattering process in a lattice of spacing $a = 1.9fm$ and mesh of $24 \times 24 \times 24$, alongside the expected phase shift δ_1 for the first two energy levels E_n in the stationary frame. The pion mass used in the lattice is $m_\pi = 480MeV$. Only the ground state ($n = 1$) and the first excited state ($n = 2$) yield energies that are allowed in the resonance limit, which is $2m_\pi < m_{resonance} < 4m_\pi$.

n	$aE_n(1)$	Expected phase (δ_1/ deg)
1	0.4559(52)	137(3)
2	0.6584(90)	170(9)

Table 1: Energy of pion-pion scattering process and the expected phase shift δ_1 for the first two energy levels E_n in the stationary frame [5]

To proceed, the energy levels E_n are converted to the momentum p_n using the momentum and energy relation in Eq. 4. These momentums are then transformed into dimensionless quantity q using Eq. 21. Subsequently, the Zeta function $\mathcal{Z}_{00}(1;q^2)$ is computed for the first two energy levels. The phase shift δ_1 can be extracted from the relation in Eq. 38.

n	$E_n(MeV)$	Momentum p (MeV)	$\lvert q\rvert$ (1)	Zeta $\mathcal{Z}_{00}(1;q^2)$ (1)	δ_1 (deg)
1	1136(13)	304(12)	0.466(19)	$-2.67(11)$	136(2)
2	1641(22)	666(14)	1.020(21)	$-42(46)$	172(8)

Table 2: Phase shifts calculations for the pion-pion scattering process in the stationary frame, with data from Table 1.

Table 2 summarizes the computed phase shifts δ_1 and intermediate values, demonstrating consistency with the expected phase shift δ_1 in Table 1. However, an important consideration in this analysis is the error propagation associated with the Zeta function. The error propagation formula requires the derivative for $\frac{d}{dq^2}$, where an analytic expression for Eq. 23 using Leskovec's method is shown below.

$$
\begin{aligned}
&\frac{d}{dq^2}\mathcal{Z}_{lm}(s=1;q^2) \\
&= \sum_{\mathbf{n}\in\mathbb{Z}^3} \mathcal{Y}_{lm}(\mathbf{n}) \frac{e^{-(\mathbf{n}^2-q^2)}}{\mathbf{n}^2-q^2}\left(1+\frac{1}{\mathbf{n}^2-q^2}\right) \\
&+ q^2 \int_0^1 e^{tq^2} \sum_{\mathbf{n}\in\mathbb{Z}^3,\mathbf{n}\neq\vec{0}} (-i)^l \mathcal{Y}_{lm}\left(\frac{\pi\mathbf{n}}{t}\right)\left(\frac{\pi}{t}\right)^{\frac{3}{2}} \exp\left(-\frac{\pi^2\mathbf{n}^2}{t}\right) dt \\
&+ \delta_{l0}\delta_{m0}\left[\frac{\pi}{2}\int_0^1 t^{-\frac{3}{2}}(e^{tq^2}-1)q^2 dt - \pi\right]
\end{aligned}
\tag{144}
$$

A limitation of this study is the restriction to only two energy levels within the resonance limit. These two energy levels and the phase shifts may not fully characterize the resonance properties comprehensively.

4 Lattice QCD in a finite volume at moving frame

In previous sections, methods for extracting phase shifts from lattice QCD simulations were discussed primarily in the context of a stationary frame. The practical limitation is that only a limited number of energy levels are physical for the scattering process.

In this section, we generalize these methods to incorporate a moving frame and particles of non-equal masses. In the moving frame, the physics is the same under the transformation of the frame, while the energy levels are shifted. Consequently, more energy levels emerge in the allowed energy region for resonance behavior, providing more data points. The non-equal mass case is particularly relevant for the scattering process like nucleon-pion or Kaon-pion scattering [26, 27].

In the moving frame (MF), where the lattice box is moving with respect to the lab frame, the total momentum of the system should obey the periodic boundary condition

$$\mathbf{P} = \mathbf{p}_1 + \mathbf{p}_2 = \frac{2\pi}{L}\mathbf{d} \quad \text{for} \quad \mathbf{d} \in \mathbb{Z}^3 \tag{145}$$

Using the Lorentz transformations, the velocity and the Lorentz factor are defined as

$$\mathbf{v} = \frac{P}{E}, \quad \gamma = \frac{1}{\sqrt{1-\mathbf{v}^2}} \tag{146}$$

The transformation between the Center of Mass Frame (CMF) and the MF is performed by the operator $\hat{\gamma}$ and its inverse $\hat{\gamma}^{-1}$

$$\hat{\gamma}\mathbf{u} = \gamma\mathbf{u}_\parallel + \mathbf{u}_\perp, \quad \hat{\gamma}^{-1}\mathbf{u} = \gamma^{-1}\mathbf{u}_\parallel + \mathbf{u}_\perp, \quad \mathbf{u}_\parallel = \frac{\mathbf{u}\cdot\mathbf{v}}{|\mathbf{v}|^2}\mathbf{v}, \quad \mathbf{u}_\perp = \mathbf{u} - \mathbf{u}_\parallel \tag{147}$$

where is $\mathbf{u}$ is an arbitrary space vector.

In the context of Lorentz transformation of the lattice box, the boost in the time direction does not affect the phase shift extraction, which relies on the dimensionless quantity q in the CMF.

The conservation of momentum in CMF is

$$\mathbf{p}^* = \mathbf{p}_1^* = -\mathbf{p}_2^* \tag{148}$$

where $\mathbf{p}^*$ is the momentum of the particle in the CMF. The momentum in the MF relates to the momentum in CMF by the Lorentz transformation

$$\mathbf{p_1} = \hat{\gamma}(\mathbf{p}^* + \mathbf{v}E_1^*) \tag{149}$$

$$\mathbf{p_2} = \hat{\gamma}(-\mathbf{p}^* + \mathbf{v}E_2^*) \tag{150}$$

The total energy relation is

$$E^* = \gamma^{-1}E = \sqrt{m_1^2 + |\mathbf{p}^*|^2} + \sqrt{m_2^2 + |\mathbf{p}^*|^2} \tag{151}$$

Here, the coefficient A is defined as

$$A \equiv 1 + \frac{m_1^2 - m_2^2}{E^{*2}} \tag{152}$$

Thus, the energy E_1 is

$$E_1 = \frac{E^*}{2}\left[1 + \frac{m_1^2 - m_2^2}{E^{*2}}\right] = \frac{E^*}{2}A \tag{153}$$

using the energy in CMF and conservation of energy.

Therefore, Eq. 150 can be rewritten as

$$\begin{aligned}
\mathbf{p}^* &= \hat{\gamma}^{-1}\mathbf{p}_1 - \mathbf{v}E_1^* && (154)\\
&= \hat{\gamma}^{-1}\left[\mathbf{p}_1 - \hat{\gamma}\mathbf{v}E_1^*\right] && (155)\\
&= \hat{\gamma}^{-1}\left[\mathbf{p}_1 - \hat{\gamma}\frac{\mathbf{P}}{E}E_1^*\right] && (156)\\
&= \hat{\gamma}^{-1}\left[\mathbf{p}_1 - \hat{\gamma}\frac{2\pi\mathbf{d}}{LE}\frac{E^*}{2}A\right] && (157)\\
&= \hat{\gamma}^{-1}\left[\mathbf{p}_1 - \frac{1}{2}A\mathbf{P}\right] && (158)
\end{aligned}$$

This relation allows for mapping the mesh in the lab frame to the mesh in the CMF, $\mathbf{r} \in P_{\mathbf{d}}$, using the dimensionless quantity q in the Eq. 21 and the quantized momentum p in Eq. 145.

$$P_{\mathbf{d}} = \left\{\mathbf{r} | \mathbf{r} = \hat{\gamma}^{-1}\left[\mathbf{n} - \frac{1}{2}A\mathbf{P}\right]\right\} \tag{159}$$

With such a transformation of the mesh, the center-of-mass wave function is transformed as well.

$$\phi_{CM}(\mathbf{r}) = (-1)^{A\mathbf{n}\cdot\mathbf{d}}\phi_{CM}(\mathbf{r} + \hat{\gamma}\mathbf{n}L) \quad \text{for all} \quad \mathbf{n} \in \mathbb{Z}^3 \tag{160}$$

This is known as a **d**-period boundary condition. The solution to this is still Green's function, which remains unchanged from the stationary frame in Section 2.1.2. However, the matrix element $M_{lm,l'm'}(q)$ requires a Lorentz factor and a mesh transformation to $\mathbf{r} \in P_{\mathbf{d}}$.

$$M^{\mathbf{d}}_{lm,l'm'}(q) = \frac{(-1)^l}{\gamma\pi^{3/2}} \sum_{j=|l-l'|}^{l+l'} \sum_{s=-j}^{j} \frac{i^j}{q^{j+1}} \mathcal{Z}^{\mathbf{d}}_{js}(1; q^2) C_{lm,js,l'm'} \tag{161}$$

where $C_{lm,js,l'm'}$ is the same tensor as in Eq. 22. The modified Zeta function in the moving frame is expressed as:

$$\mathcal{Z}^{\mathbf{d}}_{lm}(1;q^2) = \sum_{\mathbf{r}\in P_{\mathbf{d}}} \frac{\mathcal{Y}_{lm}(\mathbf{r})}{(\mathbf{r}^2-q^2)^s} \tag{162}$$

Using Leskovec's method in Section 2.2.2 to find an alternative expression for the Zeta function. Apart from the changes in mesh, the Fourier transform used from Eq. 85 to Eq. 106 has an extra factor of γ if the change of variable from $\mathbf{n}$ to $\mathbf{r}$ is applied. The alternative expression for the Zeta function in the moving frame is [10]

$$\begin{aligned}
&\mathcal{Z}^{\mathbf{d}}_{lm}(s=1;q^2) \\
&= \sum_{\mathbf{r}\in P_{\mathbf{d}}} \mathcal{Y}_{lm}(\mathbf{r}) \frac{e^{-(\mathbf{r}^2-q^2)}}{\mathbf{r}^2-q^2} && \text{Finite sum term} \\
&+ \gamma \int_0^1 e^{tq^2} \sum_{\mathbf{n}\in\mathbb{Z}^3,\mathbf{n}\neq\vec{0}} (-1)^{A\mathbf{n}\cdot\mathbf{d}} (-i)^l \mathcal{Y}_{lm}\left(\frac{\pi\hat{\gamma}[\mathbf{n}]}{t}\right)\left(\frac{\pi}{t}\right)^{\frac{3}{2}} \exp\left(-\frac{\pi^2(\hat{\gamma}[\mathbf{n}])^2}{t}\right) dt && \text{Integral term} \\
&+ \delta_{l0}\delta_{m0}\gamma\left[\frac{\pi}{2}\int_0^1 t^{-\frac{3}{2}}(e^{tq^2}-1)dt - \pi\right] && \text{Asymptotic term}
\end{aligned} \tag{163}$$

5 Application: Pion-pion scattering phase shift at moving frame

5.1 Boosted frames

Now, we consider the pion-pion scattering process in a moving frame. Specifically, we consider the following boosted frame:

5.1.1 Moving Frame 1 (MF1)

The MF1 has the periodicity vector $\mathbf{d} = (0,0,1)^T$. Using the symmetries in this frame, the leading eigenvalue of the matrix $M_{lm,l'm'}(q)$ gives the phase shift δ_1 [5]

$$\tan\delta_1(E_{CM}) = \frac{\gamma\pi^{\frac{3}{2}}q}{\mathcal{Z}^{\mathbf{d}}_{00}(1,q^2) + \frac{2}{\sqrt{5}q^2}\mathcal{Z}^{\mathbf{d}}_{20}(1,q^2)} \tag{164}$$

n	$aE_{CM}(1)$	Expected phase (δ_1/ deg)
1	0.4869(35)	4.7(0.3)
2	0.5563(98)	162(5)

Table 3: Energy of pion-pion scattering process and the expected phase shift δ_1 for the first two energy levels E_n in MF1 [5]

n	E_{CM} (MeV)	γ (1)	q (1)	$\mathcal{Z}_{00}(1;q^2)$	$\mathcal{Z}_{20}(1;q^2)$	δ_1 (deg)
1	1025(10)	1.186(4)	0.276(23)	2.571	1.718	4.6
2	1226(28)	1.133(6)	0.583(34)	−5.221	−2.465	162.6

Table 4: Phase shifts calculations for the pion-pion scattering process in MF1, with data from Table 3.

Table 4 shows the phase shifts δ_1 calculated for the first two energy levels E_{CM} in MF1. The phase shifts are consistent with the expected phase shifts in Table 3. Notably, the error propagation for the phase shifts is not included. The tangent term in 164 depends on the energy E_{CM} because both the dimensionless quantity q and the gamma factor γ depend on the energy. The error propagation is then not trivial due to the Lorentz transformation with the mesh $\mathbf{r} \in P_{\mathbf{d}}$.

To address this, the Monte Carlo (MC) method is employed, sampling the energy levels to find the distribution of the phase shift δ_1. We assume the error in energy E from the lattice simulation follows a Gaussian distribution, in particular, we use a truncated Gaussian distribution with three standard deviations to avoid possible asymptotic behavior in the Zeta function.

The MC method involves evaluating the tangent term in Eq. 164 at various input E_{CM}. This raises the computation cost for the Zeta function at adjacent energy levels. The Zeta function is smooth apart from the poles at $q^2 = \mathbf{r}^2$ and therefore the interpolation of the Zeta function is possible [25]. The interpolation can be done using the Gaussian process regressor [28, 29].

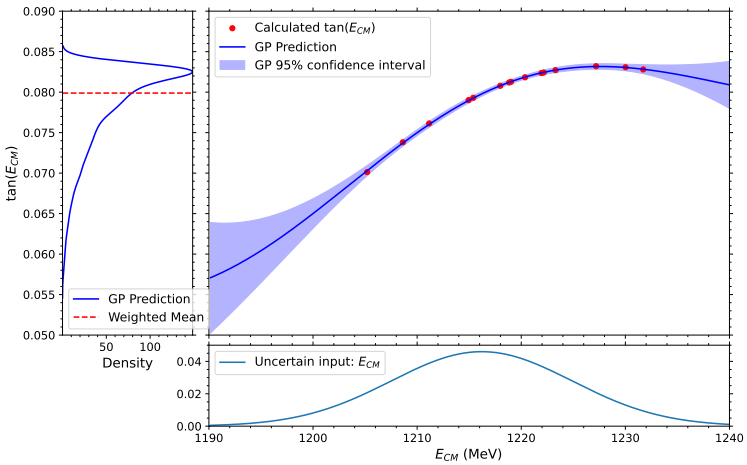

Figure 16: Gaussian process regression of the tangent term in Eq. 164 at 15 different energy levels E_{CM} in MF1.

In Fig. 16, we first evaluate the tangent term in Eq. 164 for 15 different energy levels E_{CM} in MF1. The Gaussian process regressor is then used to interpolate the tangent term at different energy levels. The regression provides a smooth function for the tangent term, and the corresponding standard deviation at each energy level is also obtained, shown in the shaded region. In practice, more points are needed to ensure the accuracy of the interpolation. The MC method is then used to sample the energy levels and find the distribution of the phase shift δ_1. The distribution of the phase shift δ_1 is asymmetric because the $\tan\delta_1$ is non-linear in the three standard deviations of the energy E_{CM}. This indicates that improvements in the precision of the energy E_{CM} are needed to reduce the uncertainty in the phase shift δ_1.

Table 5 shows the estimated error for the phase shift δ_1, confirming consistency with expected values from Table 3.

n	E_{CM} (MeV)	$\mathcal{Z}_{00}(1;q^2)$	$\mathcal{Z}_{20}(1;q^2)$	$\tan\delta_1$ (1)	δ_1 (deg)
1	1025(10)	2.7(5)	1.75(18)	0.079(4)	4.5(2)
2	1226(28)	5(1)	−2.49(28)	−0.32(7)	162(4)

Table 5: Phase shifts with Monte Carlo error propagation for the pion-pion scattering process in MF1.

5.1.2 Moving Frame 2

The MF2 has the periodicity vector $\mathbf{d} = (1,1,0)^T$. Using the symmetries in this frame, the leading eigenvalue of the matrix $M_{lm,l'm'}(q)$ gives the phase shift δ_1 [5]

$$\tan\delta_1(E_{CM}) = \frac{\gamma\pi^{\frac{3}{2}}q}{\mathcal{Z}_{00}^{\mathbf{d}}(1,q^2) - \frac{1}{\sqrt{5}q^2}\mathcal{Z}_{20}^{\mathbf{d}}(1,q^2) + i\frac{\sqrt{3}}{\sqrt{10}q^2}(\mathcal{Z}_{22}^{\mathbf{d}}(1,q^2) - \mathcal{Z}_{2,-2}^{\mathbf{d}}(1,q^2))} \tag{165}$$

The expected phase shifts for the first two energy levels E_{CM} in MF2 based on lattice simulation are shown in Table 6.

n	$aE_{CM}(1)$	Expected phase (δ_1/ deg)
1	0.5660(42)	15.3(4)
2	0.642(11)	160(6)

Table 6: Energy of pion-pion scattering process and the expected phase shift δ_1 for the first two energy levels E_n in MF2 [5]

n	E_{CM} (MeV)	γ (1)	q (1)	$\mathcal{Z}_{00}(1;q^2)$	$\mathcal{Z}_{20}(1;q^2)$	$\mathcal{Z}_{22}(1;q^2)$	δ_1 (deg)
1	1069(14)	1.322(7)	0.360(17)	1.432	-1.107	$-0.565i$	14.8(2.5)
2	1310(34)	1.224(10)	0.68(4)	9.981	-5.784	$12.67i$	162(4)

Table 7: Phase shifts calculations for the pion-pion scattering process in MF1, with data from Table 3.

Table 7 illustrates the calculated phase shift based on the nominal Zeta function. In contrast to MF1, the Monte Carlo method encounters challenges due to the asymptotic behavior of Zeta functions under three standard deviations in energy E_{CM}, impacting the expectation of the tangent term. Alternatively, one can estimate the error by using the numerical differentiation of the tangent term with respect to the energy E_{CM}. This results in an error of $\Delta\delta_1 = 369\,\text{deg}$, which is physically implausible.

5.2 Pion-pion scattering phase shift fitting result

The pion-pion scattering process involves a resonance behavior, typically modeled by the Breit-Wigner formula, which is a Lorentzian function of the energy E_{CM} with the resonance mass $m_{resonance}$ and the coupling constant g. Especially for the pion-pion scattering process, two particles of equal mass have the following relation, known as the effective range formula and is valid for the elastic region $2m_\pi < E < 4m_\pi$ [30].

$$\tan\delta_1(E_{CM}) = \frac{g^2_{\rho\pi\pi}}{6\pi}\frac{(\frac{E^2_{CM}}{4})^{\frac{3}{2}}}{E_{CM}(m^2_\rho - E^2_{CM})} \tag{166}$$

where m_ρ is the mass of the resonance ρ meson and $g_{\rho\pi\pi}$ is the coupling constant for the resonance decay into a pair of pions.

The decay with Γ is expressed in terms of $_{\rho\pi\pi}$ and m_ρ, accounting for the pion-pion phase space [31].

$$\Gamma = \frac{g^2_{\rho\pi\pi}}{6\pi}\frac{(m^2_\rho/4 - m^2_\pi)^{\frac{3}{2}}}{m^2_\rho} \tag{167}$$

Table 8 complies with the center-of-mass energy and phase shifts collected from the stationary frame, MF1 and MF2.

Frame	n	E_{CM} (MeV)	$\tan\delta_1$	δ_1(deg)
CMF	1	1139(13)	−0.99(6)	135.3(1.6)
CMF	2	1645(22)	−0.14(15)	172(8)
MF1	1	1025(10)	0.079(4)	4.53(0.21)
MF1	2	1226(28)	−0.32(7)	162(4)
MF2	1	1069(14)	0.26(5)	14.8(2.5)
MF2	2	1310(34)	−0.32(8)	162(4)

Table 8: Phase shifts calculations for the pion-pion scattering process in the stationary frame, MF1 and MF2.

Given uncertainties in both the energy and the phase shift, the fitting of the phase shift to the Breit-Wigner formula is performed using the Orthogonal Distance Regression (ODR) method [32], which is a generalization of the least squares method considering the uncertainties in both the dependent and independent variables. Instead of fitting δ_1 directly, the tangent term is more suitable for the fitting. The ODR method gives the optimal parameters and their covariance matrix

$$\begin{aligned} m_\rho &= 1111.63(8.95)\text{MeV} \\ g_{\rho\pi\pi} &= 6.31(0.44) \end{aligned} \qquad \begin{bmatrix} 80.2 & -1.13 \\ & 0.20 \end{bmatrix} \tag{168}$$

The goodness of fit metric $\chi^2/d.o.f$ yields $1.38/4 = 0.35$, suggesting an overestimation of the uncertainties in the data. This encompasses both the uncertainties in the energy obtained from the lattice simulation and during the error propagation for MF2.

Fig 17 shows the tangent term $\tan\delta_1$ with respect to energy E_{CM} for the pion-pion scattering process in the stationary frame (CMF), MF1 and MF2, with the Breit-Wigner fit curve overlaid. The tangent term $\tan\delta_1$ has the asymptotic behavior at the resonance energy m_ρ.

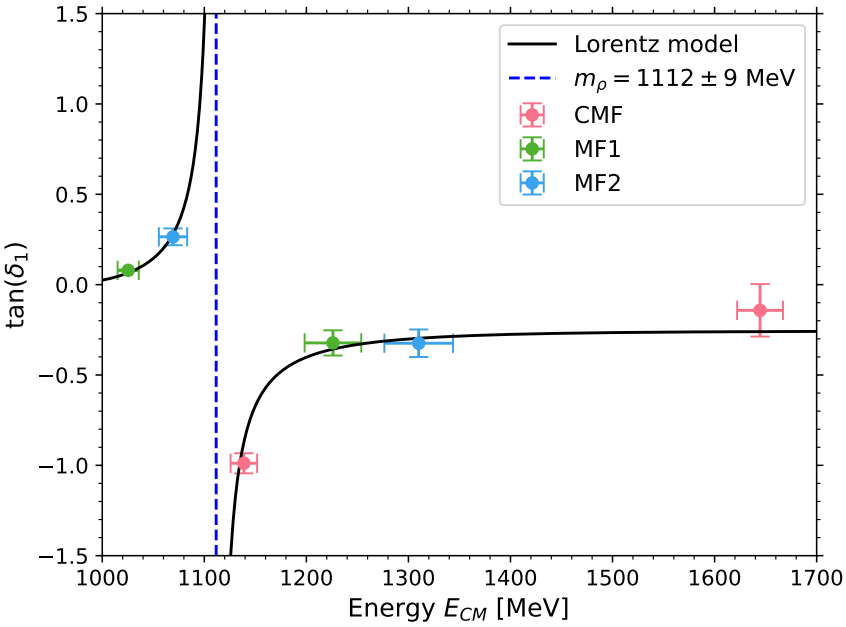

Figure 17: $\tan\delta_1$ vs E_{CM} for the pion-pion scattering process in the stationary frame (CMF), MF1 and MF2. The Breit-Wigner fit is shown in black.

The cross-section σ, a measure of the probability of the scattering process, is proportional to $\sin^2\delta_1$ [33]. Fig. 18 depicts $\sin^2\delta_1$ with respect to the energy E_{CM}, highlighting the resonance behavior in pion-pion scattering.

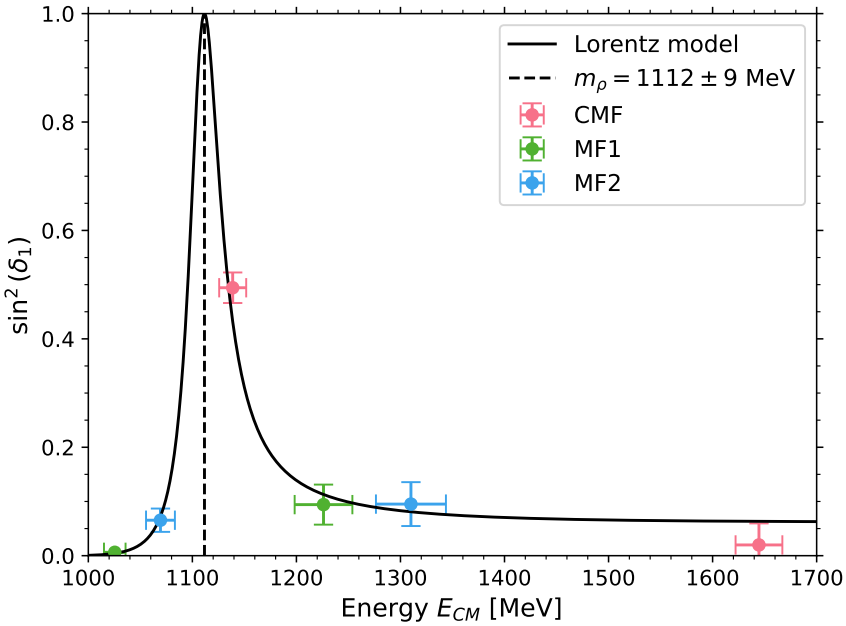

Figure 18: $\sin^2 \delta_1$ vs E_{CM} for the pion-pion scattering process in the stationary frame (CMF), MF1 and MF2.

Finally, the calculated decay width Γ calculated derived from the fit parameters and Eq. 167 is

$$\Gamma = 37.57(6.05)\text{MeV} \tag{169}$$

m_π (MeV)	m_ρ (MeV)	Γ_ρ (MeV)	$g_{\rho\pi\pi}$
480	1112(9)	37.5(6.1)	6.31(44)

Table 9: The results for the ρ-meson mass m_ρ, the decay width Γ_ρ, and the effective $\rho \to \pi\pi$ coupling $g_{\rho\pi\pi}$ at pion mass $m_\pi = 480$ Mev [5]

Table 9 summarizes results for resonance mass m_ρ, decay width Γ_ρ, and effective $\rho \to \pi\pi$ coupling $g_{\rho\pi\pi}$ at $m_\pi = 480$ MeV for the findings in [5]. The results obtained in this study are consistent with the previous findings, confirming the applicability of the Lattice QCD in the pion-pion scattering process.

We have shown the application of the Lattice QCD in the pion-pion scattering process in the moving frame. Along with the stationary frame, the enriched dataset allows for the extraction of the resonance properties. The error propagation for the phase shift is done using the Monte Carlo method and the fitting of the phase shift to the Breit-Wigner formula is done using the ODR method. The fitting yields the value for the resonance

mass m_ρ, the decay width Γ_ρ, and the effective $\rho \to \pi\pi$ coupling $g_{\rho\pi\pi}$ at pion mass $m_\pi = 480$ Mev, providing insights into the strong interaction of quarks.

6 Conclusion and outlook

In conclusion, Lattice QCD offers a robust framework to study strong interactions in a non-perturbative way by discretizing space-time. In the context of pion-pion scattering, the resonance behavior is explored through the phase shift extraction using Luscher's method, which links the finite volume energy spectrum with the infinite volume phase shift. The computational difficulties arise in the Zeta function, where the integral is coupled with a sum over the mesh. Simplification of the Zeta function and Change of variables provide efficient computation and ensure convergence.

The introduction of a moving frame enhances the dataset by providing additional data points within the interaction region. The error propagation for the phase shifts employs the Monte Carlo method for MF1 but encounters limitations for MF2 due to the asymptotic behavior. Phase shifts obtained from the stationary frame and moving frames are fitted to the Breit-Wigner formula using the ODR method, considering both uncertainties in energy E_{CM} and phase δ_1. This approach provides the resonance mass m_ρ, the decay width Γ_ρ, and the effective $\rho \to \pi\pi$ coupling $g_{\rho\pi\pi}$ in the lattice simulation of pion mass $m_\pi = 480$ MeV are obtained.

Future work includes enhancing the precision of the energy levels in the lattice simulation to improve the fit quality. Exploring simulations at different pion masses will help calculate the physical pion mass and compare it with experimental results. Extending the study to the other scattering processes, like the pion-nucleon and pion-Kaon scattering process, is crucial for understanding the behavior of the strong interaction of quarks within and beyond the Standard Model.

A Zeta functions

We present a series of Zeta functions with different partial waves l and m values in the stationary frame.

A.1 Zeta functions with $l = 8$

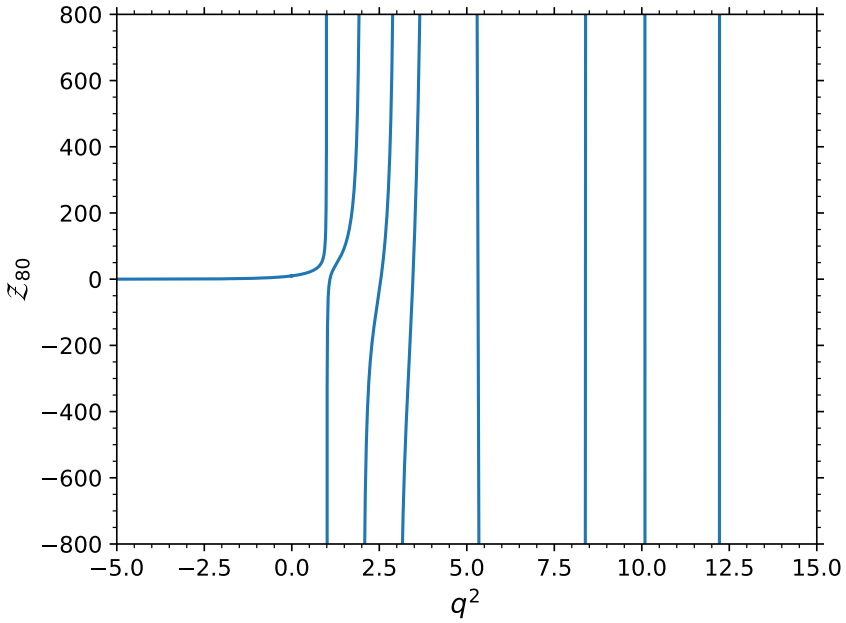

Figure 19: Plot of the Zeta function $\mathcal{Z}_{80}(1; q^2)$

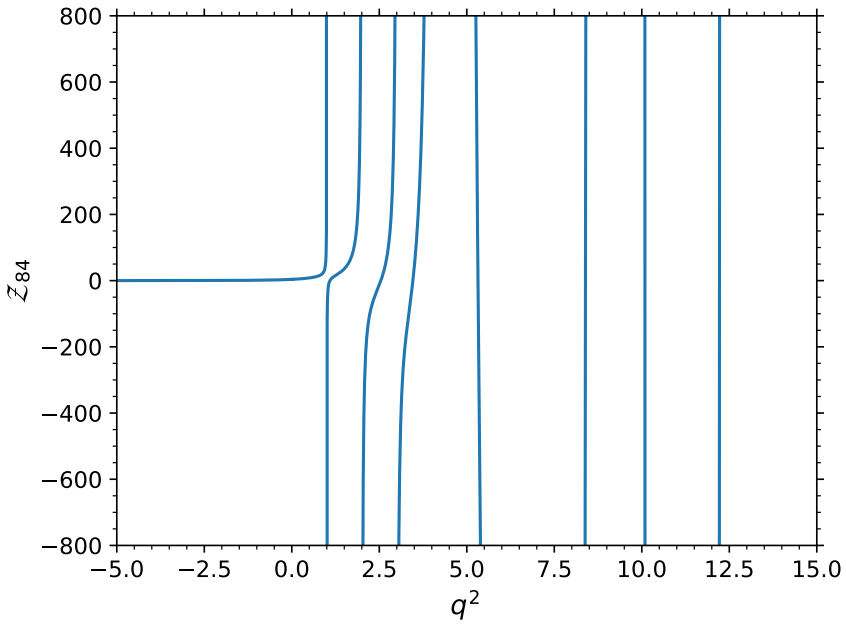

Figure 20: Plot of the Zeta function $\mathcal{Z}_{84}(1; q^2)$

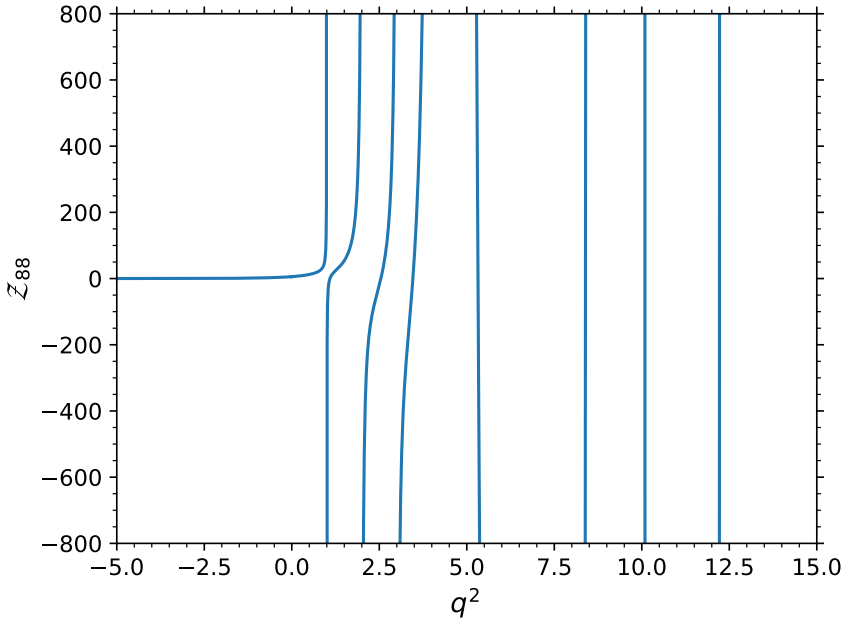

Figure 21: Plot of the Zeta function $\mathcal{Z}_{88}(1; q^2)$

A.2 Zeta functions with $l = 10$

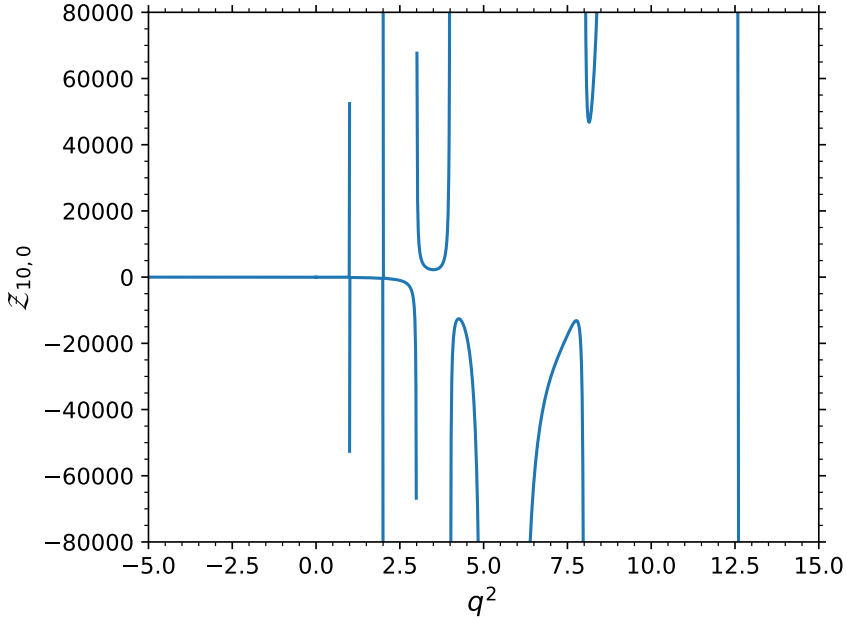

Figure 22: Plot of the Zeta function $\mathcal{Z}_{10,0}(1; q^2)$

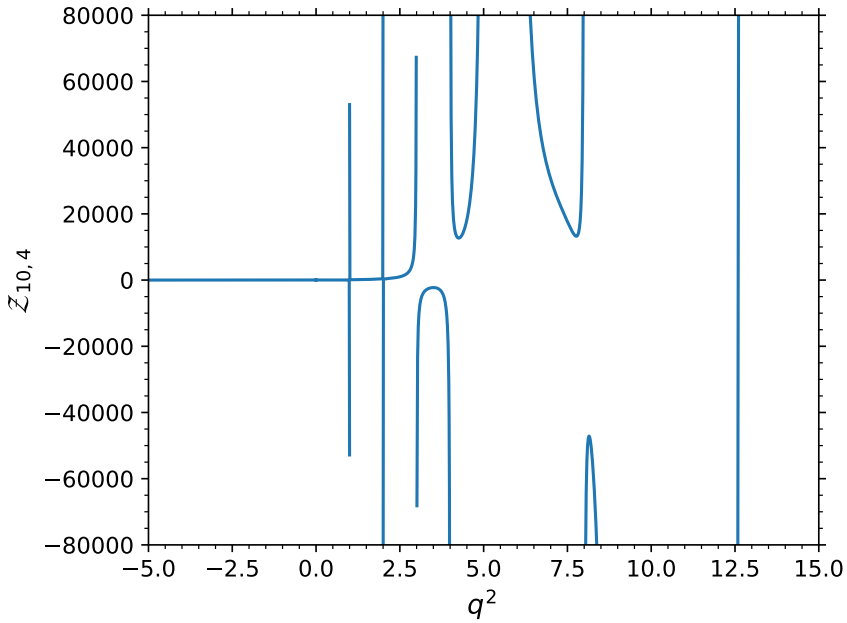

Figure 23: Plot of the Zeta function $\mathcal{Z}_{10,4}(1; q^2)$

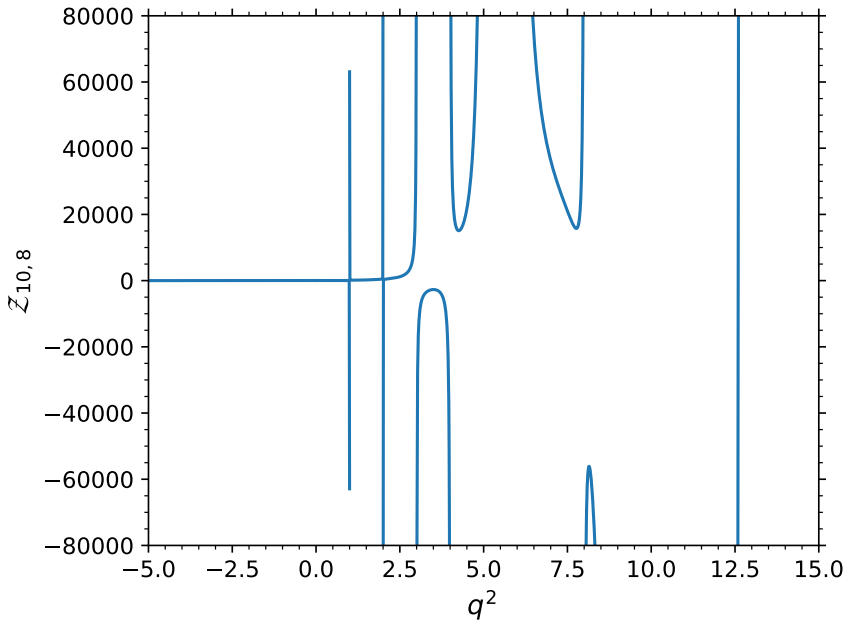

Figure 24: Plot of the Zeta function $\mathcal{Z}_{10,8}(1;q^2)$

A.3 Zeta functions with $l = 12$

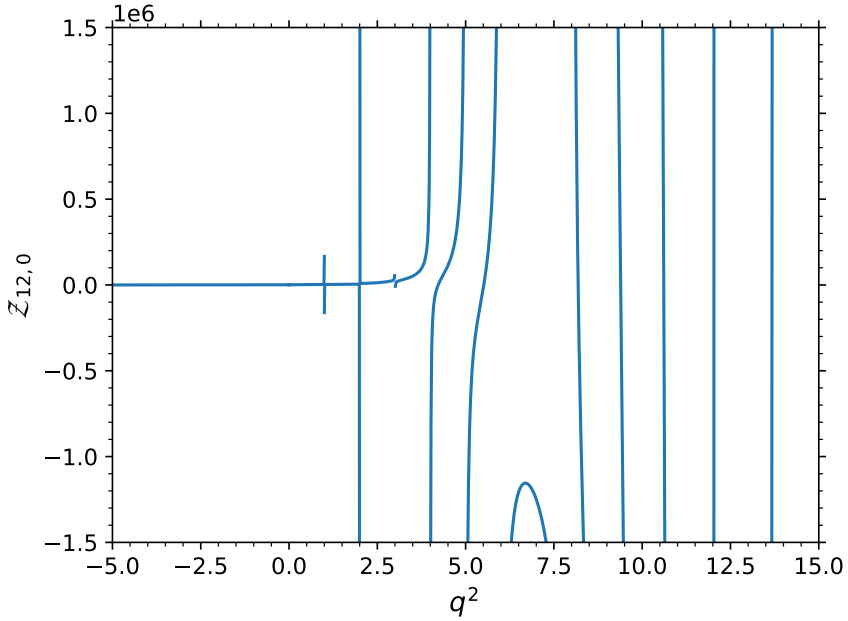

Figure 25: Plot of the Zeta function $\mathcal{Z}_{12,0}(1;q^2)$

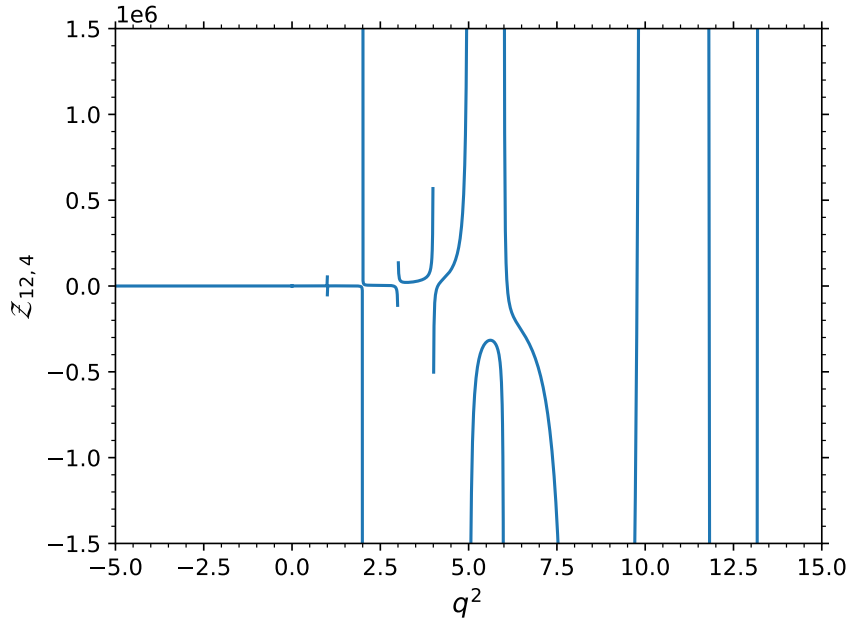

Figure 26: Plot of the Zeta function $\mathcal{Z}_{12,4}(1;q^2)$

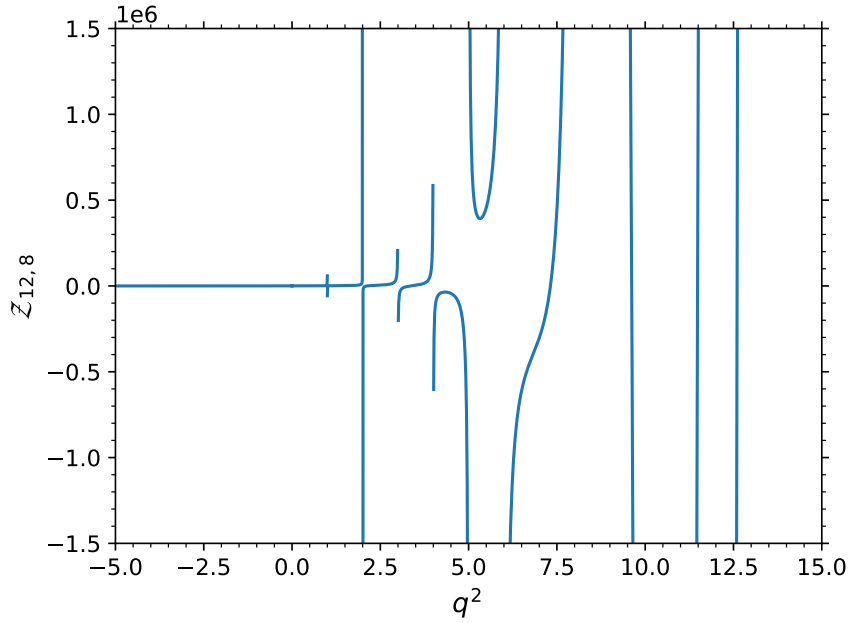

Figure 27: Plot of the Zeta function $\mathcal{Z}_{12,8}(1;q^2)$

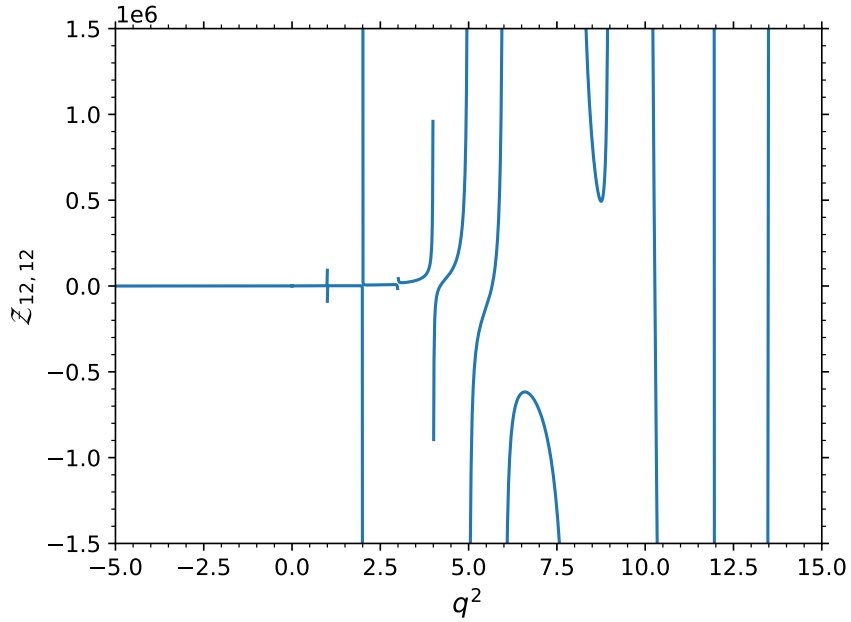

Figure 28: Plot of the Zeta function $\mathcal{Z}_{12,12}(1;q^2)$

References

[1] D. Griffiths, *Introduction to elementary particles.* John Wiley & Sons, 2020.

[2] J. Greensite, *An introduction to the confinement problem.* Springer, 2011, vol. 821.

[3] R. A. Briceño, J. J. Dudek, and R. D. Young, "Scattering processes and resonances from lattice qcd," *Reviews of Modern Physics*, vol. 90, no. 2, Apr. 2018. [Online]. Available: http://dx.doi.org/10.1103/RevModPhys.90.025001

[4] M. Luscher, "Two-particle states on a torus and their relation to the scattering matrix," *Nuclear Physics B*, vol. 354, no. 2, pp. 531–578, 1991. [Online]. Available: https://www.sciencedirect.com/science/article/pii/0550321391903666

[5] X. Feng, K. Jansen, and D. B. Renner, "Resonance parameters of the ρ meson from lattice qcd," *Phys. Rev. D*, vol. 83, p. 094505, May 2011. [Online]. Available: https://link.aps.org/doi/10.1103/PhysRevD.83.094505

[6] C. S. Pelissier, "ρ meson decay into $\pi^+\pi^-$ on asymmetrical lattices," Ph.D. Dissertation, George Washington University, 2013. [Online]. Available: https://scholarspace.library.gwu.edu/etd/kk91fk598

[7] D. J. Griffiths and D. F. Schroeter, *Introduction to Quantum Mechanics*, 3rd ed. Cambridge University Press, 2018, chapter 10.4.1 Integral Form of the Schrödinger Equation.

[8] E. T. Whittaker and G. N. Watson, *A Course of Modern Analysis*, 4th ed., ser. Cambridge Mathematical Library. Cambridge University Press, 1996.

[9] B. Zwiebach, "8.06 quantum physics iii: Lecture notes," MIT OpenCourseWare, 2018. [Online]. Available: https://ocw.mit.edu/courses/8-06-quantum-physics-iii-spring-2018/45dbd7038c3e969491eceeae86c44d42_MIT8_06S18ch7.pdf

[10] L. Leskovec and S. Prelovsek, "Scattering phase shifts for two particles of different mass and nonzero total momentum in lattice qcd," *Physical Review D*, vol. 85, no. 11, Jun. 2012. [Online]. Available: http://dx.doi.org/10.1103/PhysRevD.85.114507

[11] C. Kim, C. Sachrajda, and S. R. Sharpe, "Finite-volume effects for two-hadron states in moving frames," *Nuclear Physics B*, vol. 727, no. 1–2, p. 218–243, Oct. 2005. [Online]. Available: http://dx.doi.org/10.1016/j.nuclphysb.2005.08.029

[12] S. R. Beane, E. Chang, W. Detmold, H. W. Lin, T. C. Luu, K. Orginos, A. Parreño, M. J. Savage, A. Torok, and A. Walker-Loud, "$i = 2$ $\pi\pi$ s-wave scattering phase shift from lattice qcd," *Phys. Rev. D*, vol. 85, p. 034505, Feb 2012. [Online]. Available: https://link.aps.org/doi/10.1103/PhysRevD.85.034505

[13] C.-J. Lin, G. Martinelli, C. Sachrajda, and M. Testa, "$k \to \pi\pi$ decays in a finite volume," *Nuclear Physics B*, vol. 619, no. 1–3, p. 467–498, Dec. 2001. [Online]. Available: http://dx.doi.org/10.1016/S0550-3213(01)00495-3

[14] Z. Davoudi, "The path from finite to infinite volume: Hadronic observables from lattice qcd," 2018. [Online]. Available: https://arxiv.org/abs/1812.11899

[15] G. Colangelo and S. Dürr, "The pion mass in finite volume," *The European Physical Journal C*, vol. 33, no. 4, p. 543–553, Mar. 2004. [Online]. Available: http://dx.doi.org/10.1140/epjc/s2004-01593-y

[16] F. Williams, *Zeta Regularization.* Boston, MA: Birkhäuser Boston, 2003, ch. 15 Zeta Regularization, pp. 317–320. [Online]. Available: https://doi.org/10.1007/978-1-4612-0009-3_16

[17] N. Berline, E. Getzler, and M. Vergne, *Heat Kernels and Dirac Operators*, ser. Grundlehren Text Editions. Springer Berlin Heidelberg, 2003. [Online]. Available: https://books.google.co.uk/books?id=_e2FjvLbO94C

[18] E. Stein and R. Shakarchi, *Fourier Analysis: An Introduction.* Princeton University Press, 2003.

[19] R. Mehrem, "The plane wave expansion, infinite integrals and identities involving spherical bessel functions," 2011.

[20] D. Zwillinger, *Table of Integrals, Series, and Products.* Elsevier Science, 2014.

[21] T. Luu and M. J. Savage, "Extracting scattering phase shifts in higher partial waves from lattice qcd calculations," *Physical Review D*, vol. 83, no. 11, Jun. 2011. [Online]. Available: http://dx.doi.org/10.1103/PhysRevD.83.114508

[22] W. Detmold and M. J. Savage, "Electroweak matrix elements in the two-nucleon sector from lattice qcd," *Nuclear Physics A*, vol. 743, no. 1–3, p. 170–193, Oct. 2004. [Online]. Available: http://dx.doi.org/10.1016/j.nuclphysa.2004.07.007

[23] K. Rummukainen and S. Gottlieb, "Resonance scattering phase shifts on a non-rest-frame lattice," *Nuclear Physics B*, vol. 450, no. 1–2, p. 397–436, Sep. 1995. [Online]. Available: http://dx.doi.org/10.1016/0550-3213(95)00313-H

[24] W. Press, *Numerical Recipes 3rd Edition: The Art of Scientific Computing*, ser. Numerical Recipes: The Art of Scientific Computing. Cambridge University Press, 2007. [Online]. Available: https://books.google.co.uk/books?id=1aAOdzK3FegC

[25] M. Lüscher, "Signatures of unstable particles in finite volume," *Nuclear Physics B*, vol. 364, no. 1, pp. 237–251, 1991. [Online]. Available: https://www.sciencedirect.com/science/article/pii/055032139190584K

[26] J. Bulava, A. D. Hanlon, B. Hörz, C. Morningstar, A. Nicholson, F. Romero-López, S. Skinner, P. Vranas, and A. Walker-Loud, "Elastic nucleon-pion scattering at

m=200 mev from lattice qcd," *Nuclear Physics B*, vol. 987, p. 116105, Feb. 2023. [Online]. Available: http://dx.doi.org/10.1016/j.nuclphysb.2023.116105

[27] A. G. Nicola, J. R. de Elvira, and A. Vioque-Rodríguez, "The pion-kaon scattering amplitude and the $K_0^*(700)$ and $k^*(892)$ resonances at finite temperature," *Journal of High Energy Physics*, vol. 2023, no. 8, Aug. 2023. [Online]. Available: http://dx.doi.org/10.1007/JHEP08(2023)148

[28] J. Wang, "An intuitive tutorial to gaussian process regression," *Computing in Science and Engineering*, vol. 25, no. 4, p. 4–11, Jul. 2023. [Online]. Available: http://dx.doi.org/10.1109/MCSE.2023.3342149

[29] A. Girard, *Approximate methods for propagation of uncertainty with Gaussian process models*. University of Glasgow (United Kingdom), 2004.

[30] C. B. Lang, D. Mohler, S. Prelovsek, and M. Vidmar, "Coupled channel analysis of the ρ meson decay in lattice qcd," *Physical Review D*, vol. 84, no. 5, Sep. 2011. [Online]. Available: http://dx.doi.org/10.1103/PhysRevD.84.054503

[31] F. Renard, "Vector mesons and e+e- annihilation," *Nuclear Physics B*, vol. 82, no. 1, pp. 1–25, 1974. [Online]. Available: https://www.sciencedirect.com/science/article/pii/0550321374905768

[32] P. T. Boggs and J. E. Rogers, "Orthogonal distance regression," *Contemporary mathematics*, vol. 112, pp. 183–194, 1990.

[33] J. Taylor, *Scattering Theory: The Quantum Theory of Nonrelativistic Collisions*, ser. Dover Books on Engineering. Dover Publications, 2012. [Online]. Available: https://books.google.co.uk/books?id=OIaXvuwZMLQC